6 *pn* Junction Diode: *I–V* Characteristics

This chapter is devoted to modeling the steady state response of the *pn* junction diode. The current flowing through the diode as a function of the applied d.c. voltage, the *I–V* characteristic, is qualitatively and quantitatively correlated to the inside-the-device processes and parameters. The initial development treats the "ideal diode" and works toward the derivation of the ideal diode equation—a simple well-known *I–V* relationship. Although some of the idealizations may not be realized in practice, the ideal diode development permits unobstructed insight into the operation of the device and provides a relatively simple starting point for more exacting analyses. After comparing the ideal theory with experiment, we next focus on adjustments to the theory to correct obvious discrepancies. Several deviations from the ideal are systematically identified and explained, and appropriate modifications are introduced. Finally, we present analytical supplements to the usual analysis that will be particularly useful in subsequent chapters.

6.1 THE IDEAL DIODE EQUATION

As noted in the chapter introduction, the ideal diode is very useful for providing insight and for facilitating a base-level analysis. The *I–V* characteristics of the ideal diode are modeled by the ideal diode equation. Derivation of the equation is ostensibly the task of this section, although it should be understood that the analytical procedures, subsidiary results, and insight established in the process are really of prime importance. Making use of the *pn* junction energy band diagrams constructed in Chapter 5, we first pursue a qualitative "derivation" of the ideal diode equation. This exercise illustrates the power and utility of the energy band diagram, yielding the general form of the desired result without writing down a single mathematical relationship. Preparing for the quantitative derivation, we next detail our solution strategy. This is followed by the actual mathematical manipulations leading to the ideal diode equation. A probing examination of the final and subsidiary results concludes the section.

6.1.1 Qualitative Derivation

To set the stage, so to speak, consider the equilibrium energy band diagram for a *pn* junction shown in Fig. 6.1(a). The groups of dots (●) and circles (○) added to the figure crudely model the carrier distribution on the two sides of the junction. On the quasineutral

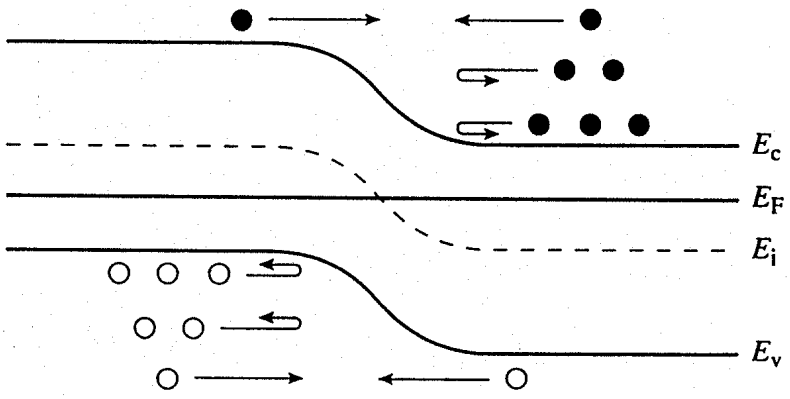

(a) Equilibrium ($V_A = 0$)

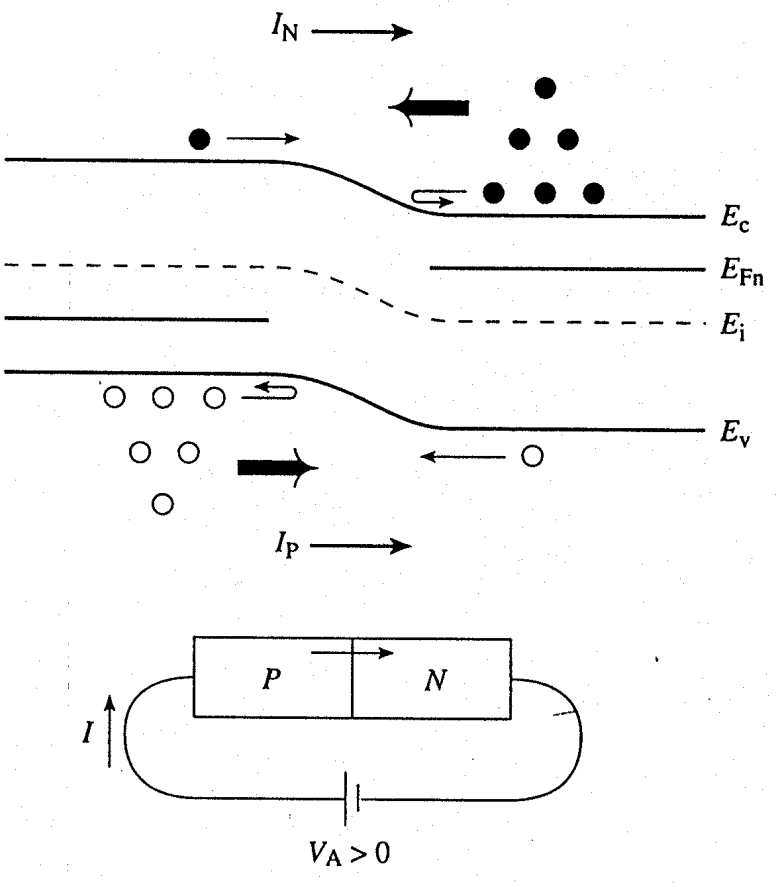

(b) Forward bias ($V_A > 0$)

Figure 6.1 *pn* junction energy band diagram, carrier distributions, and carrier activity in the near vicinity of the depletion region under (a) equilibrium ($V_A = 0$), (b) forward bias, and (c) reverse bias conditions. (d) Deduced form of the I–V characteristic.

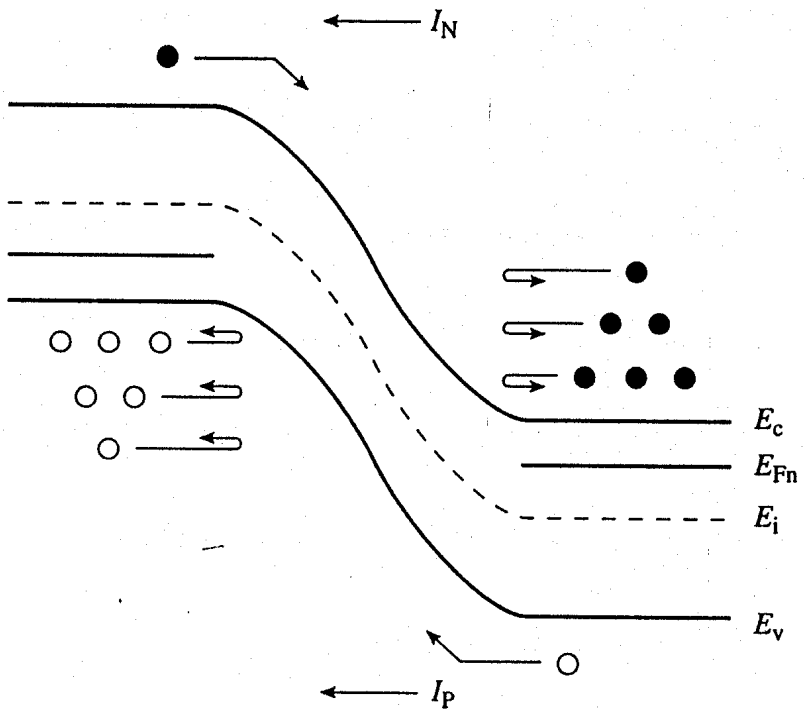

(c) Reverse bias ($V_A < 0$)

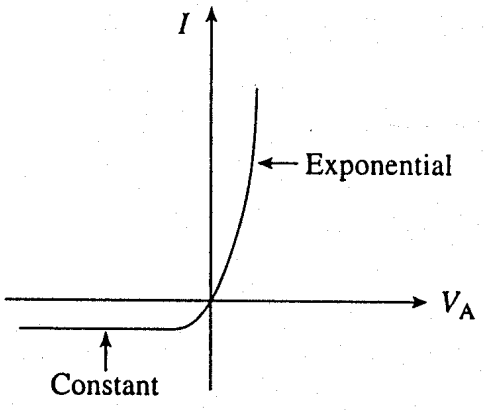

(d)

Figure 6.1 *Continued.*

n-side of the junction there are a large number of electrons and a few holes. The pyramid-like arrangement of dots (first introduced in Fig. 2.17) schematically represents the roughly exponential decrease in the electron population as one progresses upward into the conduction band. Conversely, on the quasineutral *p*-side of the junction there are a high concentration of holes and a small number of electrons. The hole population drops off in a roughly exponential fashion as one moves downward into the valence band.

The envisioned electrons and holes have thermal energy and are of course moving around inside the semiconductor. Concentrating first on the *n*-side electrons, we see that most of these carriers have insufficient energy to "climb" the potential hill. Excursions into the depletion region merely result in the lower-energy carriers being reflected back toward the *n*-side quasineutral region. However, there will be some high-energy electrons that can surmount the hill and travel over to the *p*-side of the junction. What we have been describing should be recognized as the diffusion of electrons from the high-electron population *n*-side of the junction to the low-electron population *p*-side of the junction.

Whereas electrons on the *n*-side see a potential barrier, electrons on the *p*-side are not restricted in any way. If a member of the small electron population on the *p*-side happens to wander into the depletion region, it will be rapidly swept over to the other side of the junction. Naturally, this *p*- to *n*-side drift current precisely balances the *n*- to *p*-side diffusion current under equilibrium conditions. The hole situation is completely analogous. The few *p*-side holes that have sufficient energy to surmount the potential energy barrier and gain entry to the *n*-side of the junction are precisely balanced by *n*-side holes wandering into the depletion region and being swept over to the *p*-side of the junction.

Aware of the primary carrier activity in the vicinity of the junction, let us now consider the forward bias situation pictured in Fig. 6.1(b). The most significant change relative to zero bias is a lowering of the potential hill between the *p*- and *n*-sides of the junction. The same number of minority carriers are still wandering into the depletion region and being swept over to the other side of the junction. However, with the potential hill decreased in size, more *n*-side electrons and *p*-side holes can now surmount the hill and travel to the opposite side of the junction. This gives rise to both an electron current (I_N) and a hole current (I_P) directed from the *p*-side to the *n*-side of the junction. Note from the circuit sketched below the Fig. 6.1(b) energy band diagram that the deduced current ($I = I_N + I_P$) flows in the proper direction for a forward biased diode. Moreover, because the potential hill decreases linearly with the applied forward bias and the carrier concentrations vary exponentially as one progresses away from the band edges, the number of carriers that have sufficient energy to surmount the potential barrier goes up exponentially with V_A. Thus, as summarized in Fig. 6.1(d), the forward current is expected to be an exponentially increasing function of the applied voltage.

The reverse bias situation is described by the energy band diagram in Fig. 6.1(c). Relative to equilibrium, the major effect of the bias is to increase the potential hill between the *p*- and *n*-sides of the junction. Whereas some *n*-side electrons and *p*-side holes can surmount the hill under equilibrium conditions, even a very small reverse bias, anything greater than a few kT/q in magnitude, reduces the majority carrier diffusion across the junction to a negligible level. The *p*-side electrons and *n*-side holes, on the other hand, can still wander into the depletion region and be swept to the other side of the junction. Reverse biasing thus gives rise to a current flow directed from the *n*-side to the *p*-side of the junction. Being associated with minority carriers, the reverse bias current is expected to be extremely small in magnitude. Note in addition that the minority carrier drift currents are not affected by the height of the potential hill. It is the number of minority carriers wandering into the depletion region per second that determines the current flow. (The situation is

similar to a waterfall. The water flowing over the falls is independent of the height of the falls.) Therefore, as sketched in Fig. 6.1(d), the reverse current is expected to saturate—become bias independent—once the majority carrier diffusion currents are reduced to a negligible level at a small reverse bias. If the reverse bias saturation current is taken to be $-I_0$, the overall I–V dependence is concluded to be of the general form

$$I = I_0(e^{V_A/V_{ref}} - 1) \tag{6.1}$$

Equation (6.1) is identical to the ideal diode equation if V_{ref} is set equal to kT/q.

In addition to essentially yielding the ideal diode equation, the foregoing analysis very nicely explains how a solid state diode manages to rectify a signal; i.e., how the diode passes a large current when forward biased and a very small current when reverse biased. Forward biasing reduces the potential hill between the two sides of the junction, permitting large numbers of majority carriers to be injected across the depletion region. Reverse biasing increases the potential hill, cutting off majority carrier injection and leaving only a residual current supplied by minority carriers.

Once, after completing the qualitative derivation and feeling rather smug about the insight provided, the author was asked, "Yes, but, doesn't the injection of majority carriers under forward bias and the extraction of minority carriers under reverse bias cause a charge build-up inside the device?" The immediate answer is that steady state conditions were assumed in the analysis and a charge build-up, or a change of any type, does not occur under steady state conditions. The question, however, has deeper implications. The author, concentrating solely on the carrier activity in the immediate vicinity of the depletion region, had failed to provide an overall view of carrier activity inside the device. It is the overall view that explains how injected and extracted carriers are resupplied and the status quo maintained.

In presenting the "big picture," we take the diode to be reversed biased for illustrative purposes and refer to the composite energy-band/circuit diagram shown in Fig. 6.2. The capacitor-like plates at the outer ends of the energy band diagram schematically represent the ohmic contacts to the device. The major reverse-bias activity in the immediate vicinity of the depletion region, minority carriers wandering into the depletion region and being swept to the other side of the junction, is again pictured on the diagram. Added to the diagram are E_T levels associated with R–G centers. Whenever an electron on the p-side moves to the n-side, it is replaced by an electron generated through one of the R–G centers. As pictured just to the left of the depletion region in Fig. 6.2, an electron from the valence band jumps up to the R–G center and then into the conduction band. Similarly, whenever a minority carrier hole is swept from the n-side to the p-side, the hole is quickly replaced by the carrier generation process. The electrons falling down the hill to the n-side, and the electrons simultaneously generated during the n-side replacement of lost holes, in turn give rise to an excess of majority carrier electrons on the n-side of the junction. (Two extra electrons are pictured adjacent to the depletion region on the n-side of the junction in Fig. 6.2.) The extra majority carrier electrons set up a local electric field that pushes adjacent electrons toward the contact. With great rapidity this displacement propagates until

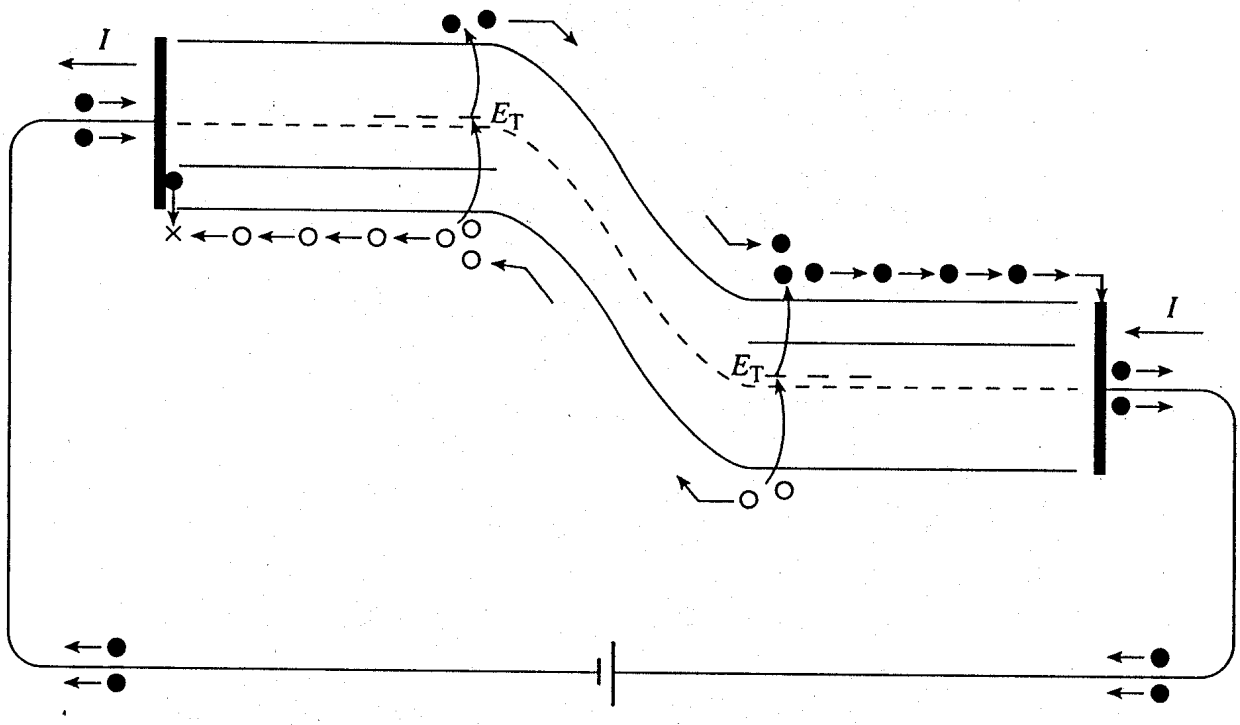

Figure 6.2 Composite energy-band/circuit diagram providing an overall view of carrier activity inside a reverse-biased *pn* junction diode. The capacitor-like plates at the outer ends of the energy band diagram schematically represent the ohmic contacts to the diode.

the entire in-line group of *n*-side electrons moves slightly toward the contact. Electrons equal in number to the excess and immediately adjacent to the contact are pushed into the contact and out into the external circuit.† The hole activity on the *p*-side of the junction is similar. The excess appearing at the depletion region edge causes in-line holes throughout the quasineutral *p*-region to move over slightly. A number of holes equal to the excess are pushed into the contact where they recombine with electrons from the metal. This recombination may be viewed as completing the circle, eliminating the extra electrons pushed into the external circuit on the *n*-side of the diode.

As a somewhat unrelated observation, it is interesting to note from Fig. 6.2 that both electrons and holes contribute to the current through the depletion region, while the hole current dominates far from the junction on the *p*-side of the device and the electron current dominates far from the junction on the *n*-side of the device. The total current through the diode must be constant, but the component electron and hole currents obviously vary with position inside the diode.

† The phenomenon just described might be likened to the real-life situation where latecomers to a party enter a room absolutely crammed with people. It is assumed there are two doors at opposite ends of the room. By forcing their way into one door, the newcomers cause a like number of people to be pushed out the other door.

6.1.2 Quantitative Solution Strategy

Going into a football game, coaches always have a game plan, a strategy for winning the game. Herein we develop and explain the strategy used in the quantitative derivation of the ideal diode equation. Although mathematical steps in the derivation are relatively few and quite straightforward, the strategy underlying the steps is rather involved and needs to be clearly understood in applying the solution approach to other problems and in implementing modifications to the theory.

General Considerations

We begin by listing the basic assumptions made in the analysis. (Additional assumptions will be necessary as the strategy unfolds.)

(1) The diode is being operated under steady state conditions.

(2) A nondegenerately doped step junction models the doping profile.

(3) The diode is one-dimensional.

(4) Low-level injection prevails in the quasineutral regions.

(5) There are no processes other than drift, diffusion, and thermal recombination–generation taking place inside the diode. Specifically, $G_L = 0$.

The preceding assumptions seem reasonable since they were all explicitly or implicitly invoked in establishing the *pn* junction electrostatics.

Let us next consider the general relationships available for computing the current. They are:

$$I = AJ \qquad (A = \text{cross-sectional area}) \tag{6.2}$$

$$J = J_N(x) + J_P(x) \tag{6.3}$$

$$J_N = q\mu_n n\mathscr{E} + qD_N\frac{dn}{dx} \tag{6.4a}$$

$$J_P = q\mu_p p\mathscr{E} - qD_P\frac{dp}{dx} \tag{6.4b}$$

Equation (6.3) reflects the fact that the total current density is constant throughout the diode, but the electron and hole components vary with position. Equations (6.4) are the one-dimensional versions of Eqs. (3.18). Clearly, if exact analytical solutions for $\mathscr{E}$, n, and p versus x were available, we would need to proceed no further. However, only an approximate three-region electrostatic solution is available, as schematically summarized in

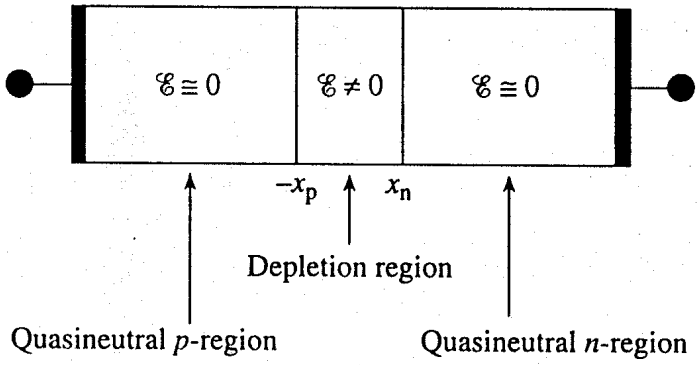

Figure 6.3 Diode electrostatic regions.

Fig. 6.3. We do note that the conditions required for the use of the minority carrier diffusion equations, including $\mathscr{E} \cong 0$ and low-level injection, are satisfied in the quasineutral regions of the diode.

Quasineutral Region Considerations

Under the assumed steady state conditions with $G_L = 0$, the minority carrier diffusion equations appropriate for the p and n quasineutral regions are

$$0 = D_N \frac{d^2 \Delta n_p}{dx^2} - \frac{\Delta n_p}{\tau_n} \quad \ldots x \leq -x_p \tag{6.5a}$$

$$0 = D_P \frac{d^2 \Delta p_n}{dx^2} - \frac{\Delta p_n}{\tau_p} \quad \ldots x \geq x_n \tag{6.5b}$$

Moreover, since $\mathscr{E} \cong 0$ and $dn_0/dx = dp_0/dx = 0$, Eqs. (6.4) for the carrier current densities in the quasineutral regions simplify to

$$J_N = qD_N \frac{d\Delta n_p}{dx} \quad \ldots x \leq -x_p \tag{6.6a}$$

$$J_P = -qD_P \frac{d\Delta p_n}{dx} \quad \ldots x \geq x_n \tag{6.6b}$$

We know the general solution to Eqs. (6.5) and it is a trivial matter to compute the carrier current densities from Eqs. (6.6). Unfortunately, the current density solutions so obtained are limited to non-overlapping segments of the diode. We can only determine $J_N(x)$ in the quasineutral p-region and $J_P(x)$ in the quasineutral n-region. To solve for J using Eq. (6.3), there must be at least one point inside the diode where one knows both

$J_N(x)$ and $J_P(x)$. Being centrally located, the depletion region is the obvious place to seek overlapping J_N and J_P solutions, solutions possibly extrapolated from the quasineutral regions.

Depletion Region Considerations

The full-blown continuity equations, Eqs. (3.46), must be used in seeking solutions for the carrier currents within the $\mathscr{E} \neq 0$ depletion region. Under the previously specified assumptions, the continuity equations simplify to

$$0 = \frac{1}{q}\frac{dJ_N}{dx} + \left.\frac{\partial n}{\partial t}\right|_{\substack{\text{thermal}\\ \text{R–G}}} \tag{6.7a}$$

$$0 = -\frac{1}{q}\frac{dJ_P}{dx} + \left.\frac{\partial p}{\partial t}\right|_{\substack{\text{thermal}\\ \text{R–G}}} \tag{6.7b}$$

Suppose the additional assumption is now made that *thermal recombination–generation is negligible throughout the depletion region;* i.e., $\partial n/\partial t|_{\text{thermal R–G}}$ and $\partial p/\partial t|_{\text{thermal R–G}}$ are arbitrarily set equal to zero in Eqs. (6.7). Eliminating the R–G terms in Eqs. (6.7) yields $dJ_N/dx = 0$ and $dJ_P/dx = 0$. J_N and J_P are therefore determined to be constants independent of position inside the depletion region under the stated assumption. The constancy of the carrier currents throughout the depletion region (including the edges) in turn allows one to write

$$J_N(-x_p \leq x \leq x_n) = J_N(-x_p) \tag{6.8a}$$

$$J_P(-x_p \leq x \leq x_n) = J_P(x_n) \tag{6.8b}$$

$J_N(-x_p)$ and $J_P(x_n)$ can be deduced of course from the quasineutral region solutions evaluated at the edges of the depletion region. Summing the J_N and J_P solutions in the depletion region then gives

$$\boxed{J = J_N(-x_p) + J_P(x_n)} \tag{6.9}$$

Clearly a solution strategy has been formulated: to solve for the minority carrier current densities in the quasineutral regions, evaluate the current densities at the depletion region edges, add the edge current densities together, and finally multiply by A to obtain the current.

The rather critical assumption that thermal recombination–generation is negligible in the depletion region can be viewed as a defining property of the ideal diode. There is

absolutely no *a priori* justification for the assumption other than it leads to a simple solution for the total current flowing in the diode. The validity of the assumption as far as real diodes are concerned will be considered when comparing theory and experiment.

Boundary Conditions

There is one more matter to address. Two boundary conditions each are required in solving Eqs. (6.5a) and (6.5b) for Δn_p and Δp_n in the p- and n-side quasineutral regions. In particular, as summarized in Fig. 6.4(a), Δn_p and Δp_n must be specified at the ohmic contacts and at the edges of the depletion region.

At the Ohmic Contacts

The ideal diode is usually taken to be a "wide-base" diode, or a diode whose contacts are several minority carrier diffusion lengths or more from the edges of the depletion region. In a wide-base diode any perturbation in the carrier concentrations created at the edges of the depletion region will decay to zero before reaching the contacts. The contacts may effectively be viewed as being positioned at $x = \pm\infty$. Thus, in the mathematical derivation

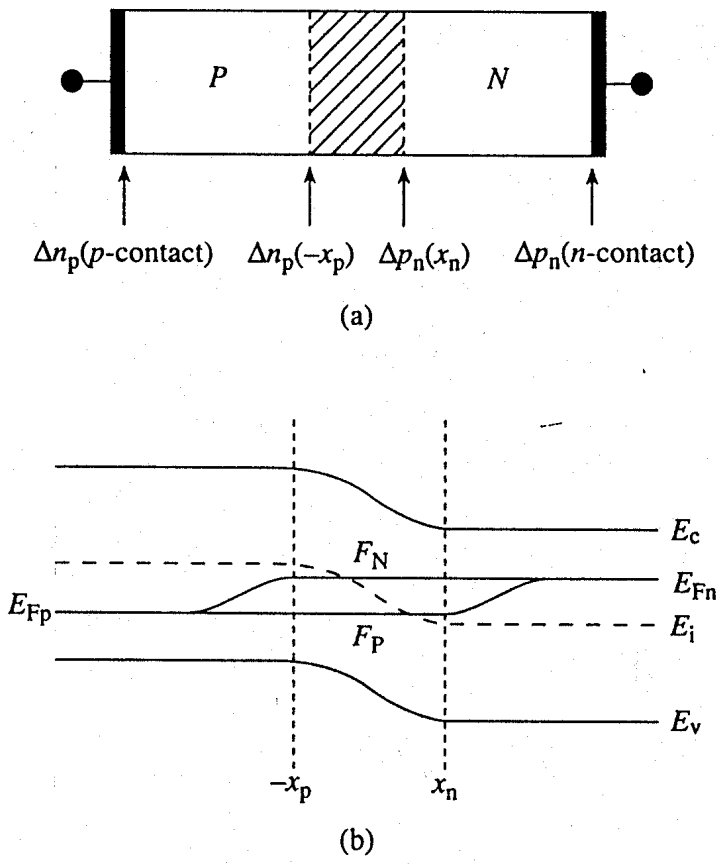

Figure 6.4 Boundary-condition related considerations. (a) Boundary positions and required values. (b) Approximate variation of the quasi-Fermi levels with position inside a forward-biased diode.

the boundary conditions to be employed are

$$\boxed{\Delta n_p(x \to -\infty) = 0} \tag{6.10a}$$

$$\boxed{\Delta p_n(x \to +\infty) = 0} \tag{6.10b}$$

At the Depletion Region Edges

To establish the boundary conditions at the edges of the depletion region, we make use of the quasi-Fermi level formalism. Equations (3.72) are the defining equations for the electron quasi-Fermi level, F_N, and hole quasi-Fermi level, F_P. If the left- and right-hand sides of the exponential versions of Eqs. (3.72a) and (3.72b) are multiplied together, one obtains

$$np = n_i^2 e^{(F_N - F_P)/kT} \tag{6.11}$$

The Eq. (6.11) relationship is valid throughout the diode under arbitrary operating conditions. Generally speaking, one does not know the variation of the quasi-Fermi levels as a function of position prior to solving for the carrier concentrations inside the diode. However, as envisioned in Fig. 6.4(b), it is reasonable to assume the F_N and F_P levels will vary monotonically from E_{Fp} far on the p-side of the junction to E_{Fn} far on the n-side of the junction. Note from Fig. 6.4(b) that the monotonic variation in the levels in turn makes $F_N - F_P \leq E_{Fn} - E_{Fp} = qV_A$ at all points inside the diode. If the equal sign in the preceding expression for $F_N - F_P$ is assumed to hold throughout the depletion region, one concludes

$$\boxed{np = n_i^2 e^{qV_A/kT} \quad \ldots -x_p \leq x \leq x_n} \tag{6.12}$$

Eq. (6.12) has been referred to as the "law of the junction." Evaluating Eq. (6.12) at the depletion region edges very rapidly leads to the desired boundary conditions. Specifically, evaluating Eq. (6.12) at the p-edge of the depletion region gives

$$n(-x_p)p(-x_p) = n(-x_p)N_A = n_i^2 e^{qV_A/kT} \tag{6.13}$$

or

$$n(-x_p) = \frac{n_i^2}{N_A} e^{qV_A/kT} \tag{6.14}$$

and

$$\boxed{\Delta n_p(-x_p) = \frac{n_i^2}{N_A}(e^{qV_A/kT} - 1)} \tag{6.15}$$

Similarly,

$$n(x_n)p(x_n) = p(x_n)N_D = n_i^2 e^{qV_A/kT} \tag{6.16}$$

or

$$p(x_n) = \frac{n_i^2}{N_D} e^{qV_A/kT} \tag{6.17}$$

and

$$\boxed{\Delta p_n(x_n) = \frac{n_i^2}{N_D}(e^{qV_A/kT} - 1)} \tag{6.18}$$

The assumption that $F_N - F_P = qV_A$ throughout the depletion region, or equivalently, assuming the quasi-Fermi levels are constant at $F_N = E_{Fn}$ and $F_P = E_{Fp}$ within the depletion region, is obviously central to obtaining the depletion-edge boundary conditions and critical to the overall analysis. Rather lengthy subsidiary analyses and a comparison with experiment indicate the assumption is typically justified.†

"Game Plan" Summary

To obtain an analytical solution for the current flowing in an ideal diode as a function of the applied voltage, proceed as follows:

(1) Solve the minority carrier diffusion equations (Eqs. 6.5) employing the (6.10) and (6.15/6.18) boundary conditions to obtain Δn_p and Δp_n in the quasineutral regions.

(2) Compute the minority carrier current densities in the quasineutral regions using Eqs. (6.6).

(3) Per Eq. (6.9), evaluate the quasineutral region solutions for $J_N(x)$ and $J_P(x)$ at the edges of the depletion region and then sum the two edge-current densities. Finally, multiply the result by the cross-sectional area of the diode.

---

† Assuming F_N and F_P are approximately constant across the depletion region is equivalent to assuming $J_N \cong 0$ and $J_P \cong 0$ within the depletion region (see Eqs. 3.76). The $J_N = 0$ and $J_P = 0$ assumption is used by some authors in an alternative derivation of the depletion-edge boundary conditions that closely parallels the V_{bi} derivation in Subsection 5.1.4. Like the constant quasi-Fermi assumption, and contrary to statements in some texts, there is really no simple a priori justification of the $J_N = 0$ and $J_P = 0$ assumption.

6.1.3 Derivation Proper

In implementing the solution procedure, let us first work with holes on the quasineutral *n*-side of the junction. To simplify the mathematics in solving Eq. (6.5b), it is convenient to shift the origin of coordinates to the *n*-edge of the depletion region as shown in Fig. 6.5(a). In terms of the translated x'-coordinate, we must solve

$$0 = D_P \frac{d^2 \Delta p_n}{dx'^2} - \frac{\Delta p_n}{\tau_p} \qquad \ldots x' \geq 0 \tag{6.19}$$

subject to the boundary conditions

$$\Delta p_n(x' \to \infty) = 0 \tag{6.20a}$$

$$\Delta p_n(x' = 0) = \frac{n_i^2}{N_D}(e^{qV_A/kT} - 1) \tag{6.20b}$$

Eq. (6.19) is one of the special-case diffusion equations listed in Table 3.2. The general solution (solution no. 1 in Table 3.2) is

$$\Delta p_n(x') = A_1 e^{-x'/L_P} + A_2 e^{x'/L_P} \qquad \ldots x' \geq 0 \tag{6.21}$$

where

$$L_P = \sqrt{D_P \tau_p} \tag{6.22}$$

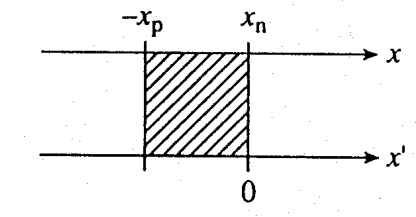

(a)

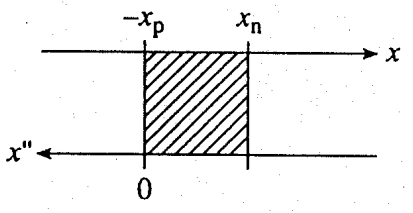

(b)

Figure 6.5 Graphical definition of the (a) x'- and (b) x''-coordinate systems.

Because $\exp(x'/L_p) \to \infty$ as $x' \to \infty$, the only way that the Eq. (6.20a) boundary condition can be satisfied is for A_2 to be identically zero. With $A_2 = 0$, application of the Eq. (6.20b) boundary condition yields $A_1 = \Delta p_n(x' = 0)$. We therefore conclude

$$\boxed{\Delta p_n(x') = \frac{n_i^2}{N_D}(e^{qV_A/kT} - 1)e^{-x'/L_P}} \quad \ldots x' \geq 0 \tag{6.23}$$

and

$$\boxed{J_P(x') = -qD_P\frac{d\Delta p_n}{dx'} = q\frac{D_P}{L_P}\frac{n_i^2}{N_D}(e^{qV_A/kT} - 1)e^{-x'/L_P}} \quad \ldots x' \geq 0 \tag{6.24}$$

On the quasineutral p-side of the junction with the x''-coordinate as defined in Fig. 6.5(b), one obtains the analogous solutions

$$\boxed{\Delta n_p(x'') = \frac{n_i^2}{N_A}(e^{qV_A/kT} - 1)e^{-x''/L_N}} \quad \ldots x'' \geq 0 \tag{6.25}$$

and

$$\boxed{J_N(x'') = -qD_N\frac{d\Delta n_p}{dx''} = q\frac{D_N}{L_N}\frac{n_i^2}{N_A}(e^{qV_A/kT} - 1)e^{-x''/L_N}} \quad \ldots x'' \geq 0 \tag{6.26}$$

All that remains is to evaluate Eqs. (6.24) and (6.26) at the depletion region edges, sum the results, and multiply by A. We find

$$J_N(x=-x_p) = J_N(x''=0) = q\frac{D_N}{L_N}\frac{n_i^2}{N_A}(e^{qV_A/kT} - 1) \tag{6.27a}$$

$$J_P(x=x_n) = J_P(x'=0) = q\frac{D_P}{L_P}\frac{n_i^2}{N_D}(e^{qV_A/kT} - 1) \tag{6.27b}$$

and

$$I = AJ = qA\left(\frac{D_N}{L_N}\frac{n_i^2}{N_A} + \frac{D_P}{L_P}\frac{n_i^2}{N_D}\right)(e^{qV_A/kT} - 1) \tag{6.28}$$

or

$$I = I_0(e^{qV_A/kT} - 1) \tag{6.29}$$

$$I_0 \equiv qA\left(\frac{D_N}{L_N}\frac{n_i^2}{N_A} + \frac{D_P}{L_P}\frac{n_i^2}{N_D}\right) \tag{6.30}$$

Equation (6.29) is the ideal diode equation. It is also sometimes referred to as the Shockley equation.

6.1.4 Examination of Results

It is worthwhile at this point to pause and examine the final and intermediate results of the derivation. We hope to become more familiar with the results while simultaneously gaining deeper insight into the operation of the *pn* junction diode. Working backward through the derivation, we first examine the ideal diode equation and the associated saturation current. Subsequently we investigate the carrier currents and carrier concentrations inside the diode. Several exercises are also presented to supplement the discussion.

Ideal *I–V*

The major features of the predicted *I–V* characteristics are summarized in Fig. 6.6. For reverse biases greater than a few kT/q, a few tenths of a volt at room temperature, the exponential voltage term in the ideal diode equation becomes negligible and $I \to -I_0$. According to the ideal diode theory, this saturation current would be observed for reverse voltages of unlimited magnitude. For forward biasing greater than a few kT/q, the exponential term dominates and $I \to I_0 \exp(qV_A/kT)$. Reflecting the expected exponential dependence, the forward-bias characteristics are often plotted on a semilog scale as illustrated in Fig. 6.6(b). Since

$$\ln(I) = \ln(I_0) + \frac{q}{kT}V_A \quad \ldots \text{ if } V_A > \text{few } \frac{kT}{q} \tag{6.31}$$

the ideal theory predicts a $V_A > 0$ semilog plot that has a linear region slope of q/kT and an extrapolated intercept of $\ln(I_0)$.

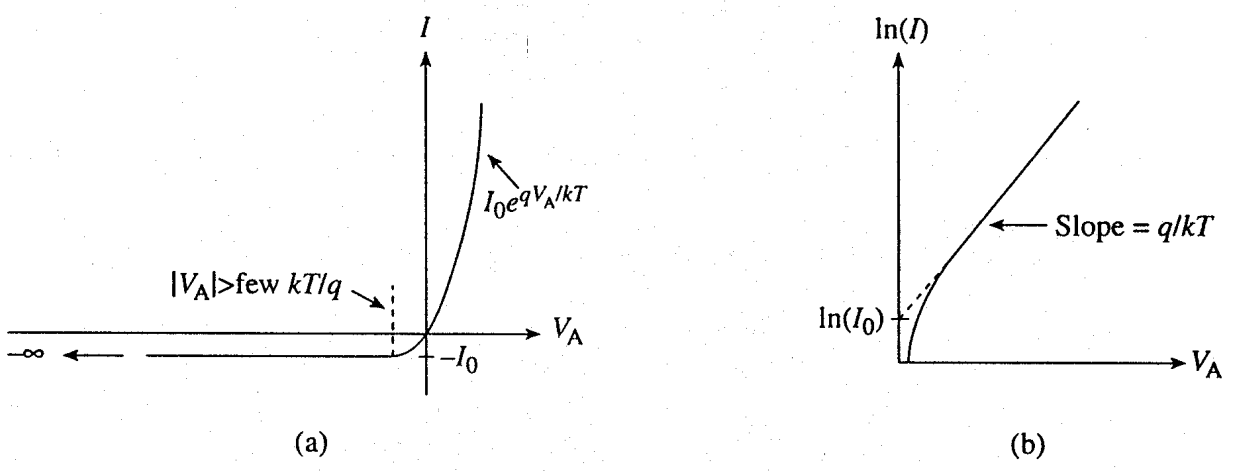

Figure 6.6 Ideal diode I–V characteristics: (a) linear plot identifying major features; (b) forward-bias semilog plot.

The Saturation Current

Two rather significant observations can be made concerning the saturation current. First, the size of I_0 can vary by many orders of magnitude depending on the semiconductor used to fabricate the diode. This strong material dependence enters through the n_i^2 factor in the I_0 expression. At room temperature $n_i = 10^{10}/\text{cm}^3$ in Si while $n_i \cong 10^{13}/\text{cm}^3$ in Ge. Thus, Ge diodes are expected to exhibit a reverse-bias saturation current roughly 10^6 times larger than that of comparable Si diodes!

The second observation relates to asymmetrically doped junctions. The I_0 expression has two terms that vary inversely with the dopings respectively on the p- and n-side of the junction. Because of the cited doping dependence, the term associated with the heavily doped side of p^+-n and n^+-p junctions becomes negligible; i.e.,

$$I_0 \cong qA \frac{D_P}{L_P} \frac{n_i^2}{N_D} \quad \ldots p^+\text{-}n\text{-diodes} \tag{6.32a}$$

and

$$I_0 \cong qA \frac{D_N}{L_N} \frac{n_i^2}{N_A} \quad \ldots n^+\text{-}p \text{ diodes} \tag{6.32b}$$

In essence, one has to consider only the lightly doped side of such junctions in working out the diode I–V characteristics. We also found one can all but neglect the heavily doped side of asymmetrical junctions in computing the depletion width and other electrostatic vari-

ables. These similar conclusions suggest that, *as a general rule, the heavily doped side of an asymmetrical junction can be ignored in determining the electrical characteristics of the junction.* If an asymmetrical junction is specified in a problem statement or at the beginning of an analysis, it should be understood that the heavily doped side is to be ignored in completing the problem or analysis.

We might mention that it is rather fortuitous that the current contribution from the heavily doped side of asymmetrical junctions is negligible. In most real diodes the p^+- or n^+-side doping is degenerate. If the current contribution from the heavily doped side were significant, comparison with experiment would necessitate a modification of the ideal diode theory to account for the degenerate doping.

Exercise 6.1

P: Two ideal p^+-n step junction diodes maintained at room temperature are identical except that $N_{D1} = 10^{15}/\text{cm}^3$ and $N_{D2} = 10^{16}/\text{cm}^3$. Compare the I–V characteristics of the two diodes; sketch both characteristics on a single set of axes.

S: For p^+-n diodes

$$I_0 \cong qA\frac{D_P}{L_P}\frac{n_i^2}{N_D}$$

Also

$$\frac{D_P}{L_P} = \sqrt{\frac{D_P}{\tau_p}} = \sqrt{\frac{(kT/q)\mu_p}{\tau_p}}$$

$\tau_{p1} = \tau_{p2}$, since the R–G center concentrations are taken to be identical in the two diodes. Moreover, although the semiconductor material is not specified in the problem statement, there is only a small difference between the $N_D = 10^{15}/\text{cm}^3$ and $N_D = 10^{16}/\text{cm}^3$ mobilities in most materials (see Fig. 3.5). Thus

$$\frac{I_{01}}{I_{02}} = \frac{N_{D2}}{N_{D1}}\sqrt{\frac{\mu_{p1}}{\mu_{p2}}} \cong 10$$

The diode 1 current is approximately ten times larger than the diode 2 current for all applied voltages (see Fig. E6.1).

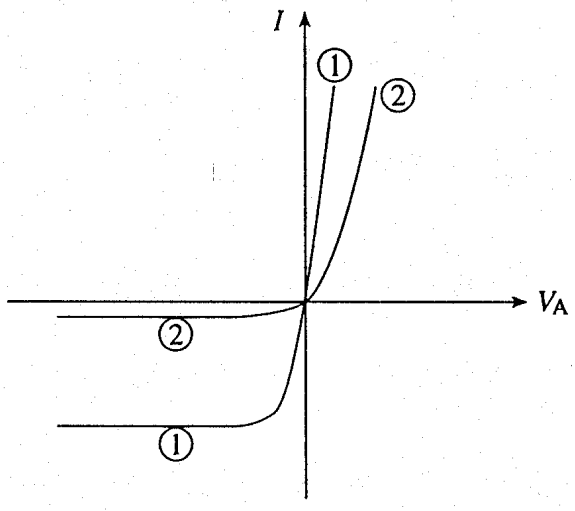

Figure E6.1

(C) Exercise 6.2

P: An *ideal* Si p^+-n step junction diode is maintained at 300 K. The diode has a cross-sectional area $A = 10^{-4}$ cm^2 and $\tau_p = 10^{-6}$ sec. Using the empirical-fit relationship for the hole mobility introduced in Exercise 3.1, write a MATLAB program that computes and plots the ideal I–V characteristic of the diode. The n-side donor doping is to be considered an input variable. Employ a linear plot with the MATLAB `axis` function set to $[-1, 0.2, -2*I_0, 5*I_0]$, where I_0 is the reverse bias saturation current. Generally use your program to explore how the ideal diode characteristic varies as a function of the semiconductor doping.

S: The program that follows was written to handle multiple doping inputs. Enclosing your input in square brackets, simply type the desired doping values separated by spaces in response to the "ND= " prompt. The sample plot (Fig. E6.2) exhibits the same general doping dependence noted in Exercise 6.1. However, examining the numerical I_0 values sent by the program to the *Command*-window, one finds a noticeable mobility dependence because of the higher assumed dopings. The user should also take note of the extremely small size of the computed saturation currents.

MATLAB program script...

```
%Variation of Ideal-Diode I-V with semiconductor doping.
%Si step junction, T = 300K.
%In response to the "ND=" prompt type [ND1 ND2 ...] to input
%multiple doping values.

%Initialization and Universal Constants
clear
k=8.617e-5;
q=1.6e-19;
```

```
%Device, Material, and System Parameters
A=1.0e-4;
ni=1.0e10;
taup=1.0e-6;
ND=input('Input the n-side doping concentration, ND=');
T=300;

%Hole Mobility Calculation
NAref=2.35e17;
μpmin=54.3;
μp0=406.9;
ap=0.88;
μp=μpmin+μp0./(1+(ND./NAref).^ap);
%The mobility calculation here assumes the hole minority carrier
  %mobility is equal to the hole majority carrier mobility.

%I-V Calculation
VA=linspace(-1,0.2);
DP=k.*T.*μp;
LP=sqrt(DP.*taup);
I0=q.*A.*(DP./LP).*(ni^2 ./ND)
I=I0.'*(exp(VA./(k.*T))-1);

%Plotting Result
close
plot(VA,I); grid;
ymin=-2*I0(1); ymax=5*I0(1);
axis([-1,0.2,ymin,ymax]);
xlabel('VA (volts)'); ylabel('I (amps)');

%Adding axes,key
xx=[-1 0.2]; yx=[0 0];
xy=[0 0]; yy=[ymin,ymax];
hold on
plot(xx,yx,'-w',xy,yy,'-w');
j=length(ND);
for i=1:j;
    yput=(0.70-0.06*i)*ymax;
    yk(i,1)=yput; yk(i,2)=yput;
    text(-0.68,(0.69-0.06*i)*ymax,['ND=',num2str(ND(i),'/cm3']);
end
xk=[-0.8 -0.7];
plot(xk,yk);
text(-0.74,0.75*ymax,'Si, 300K');
hold off
```

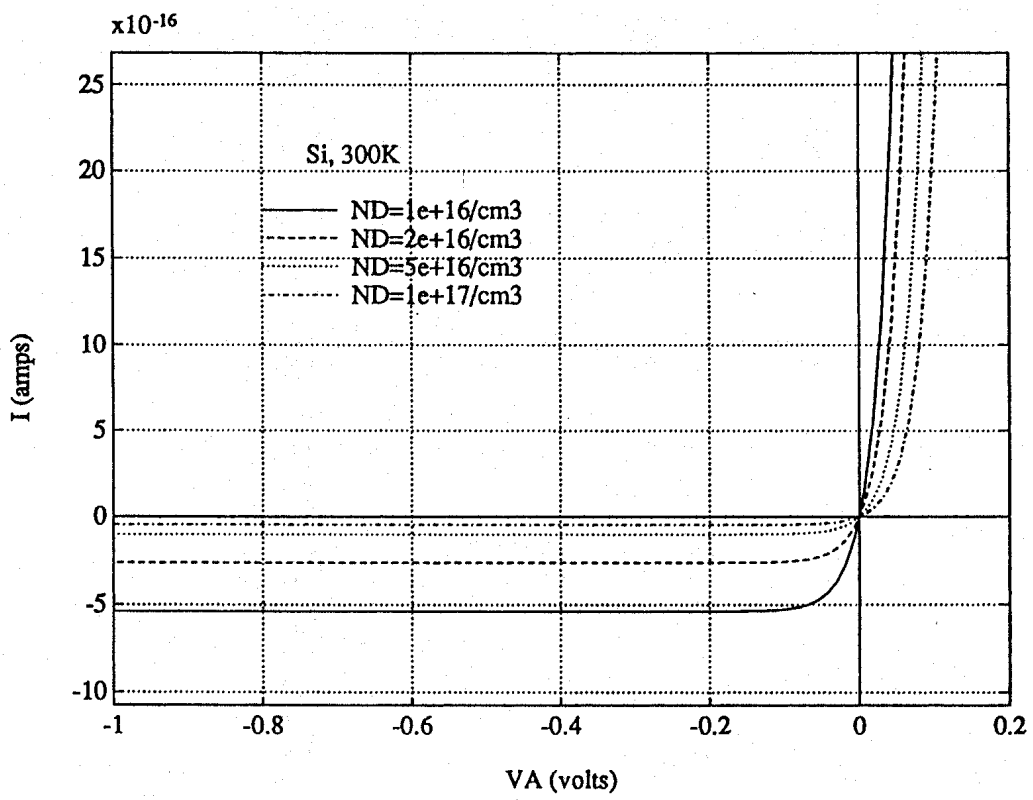

Figure E6.2

Carrier Currents

A sample plot of the carrier and total current densities as a function of position inside a forward-biased diode is displayed in Fig. 6.7. A reverse-bias plot is essentially identical except all current densities are negative. Steps in the construction of the Fig. 6.7 plot are as follows: Examining Eqs. (6.24) and (6.26), one concludes the minority carrier current densities in the quasineutral regions decay exponentially away from the edges of the depletion region. Within the depletion region, J_N and J_P per Eq. (6.8) are next drawn constant at their respective depletion-edge values. The total current density in the depletion region is then just the graphical sum of J_N and J_P. Since the total current density is constant everywhere inside the diode, the value deduced for the depletion region can be extended throughout the diode. Finally, the majority-carrier current densities in the quasineutral regions are obtained by graphically subtracting the minority-carrier current densities from the total current density.

The construction of Fig. 6.7 shows that there is sufficient information available to deduce the current densities everywhere inside the diode. Moreover, the plot helps one visualize the nature of the $J_N(x)$ and $J_P(x)$ solutions. The general form of the solutions, we might note, is consistent with the observation made at the end of the qualitative derivation. Whereas electrons and holes both contribute to the current through the depletion region, the hole current dominates far from the junction on the p-side of the device and the electron current dominates far from the junction on the n-side of the device.

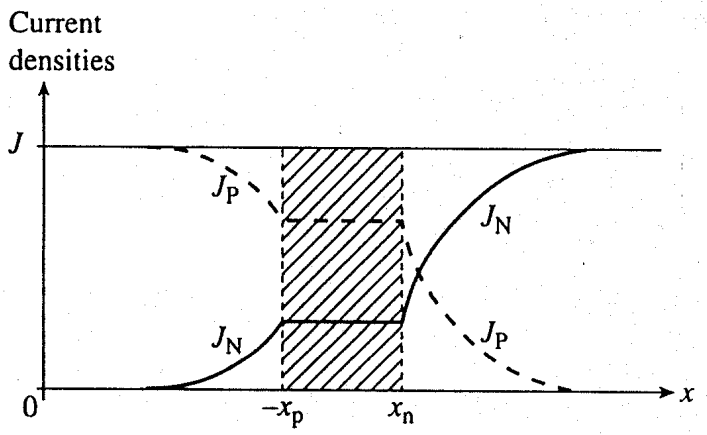

Figure 6.7 Carrier and total current densities versus position inside a forward-biased *pn* junction diode.

Carrier Concentrations

Equations (6.23) and (6.25) specify the deviation from equilibrium of the minority carrier concentrations in the quasineutral regions. From these solutions we conclude forward biasing increases the carrier concentrations over their respective equilibrium values and that reverse biasing lowers the concentrations below the equilibrium values. In either case, the perturbations decay exponentially as one proceeds away from the edges of the depletion region. Moreover, after several diffusion lengths the perturbations effectively die out and the minority carrier concentrations approach their equilibrium values; i.e., $n_p \to n_{p0} = n_i^2/N_A$ as $x \to -\infty$ and $p_n \to p_{n0} = n_i^2/N_D$ as $x \to +\infty$ independent of the applied bias. Because low-level injection is assumed to prevail in the quasineutral regions, we can also assert that the *majority* carrier concentrations in these regions are everywhere approximately equal to their equilibrium values regardless of the applied bias. Plots of the forward- and reverse-bias carrier concentrations incorporating the foregoing information are shown in Fig. 6.8. Note that the exponential decays of Δn_p and Δp_n show up as straight lines on the forward-bias plot because the carrier concentrations are being plotted on a logarithmic scale.

Under forward biasing the majority carriers are injected in large numbers over the potential hill to the other side of the junction. Once on the other side of the junction, the injected carriers become minority carriers and are progressively eliminated by recombination as they attempt to diffuse deeper into the region. (The situation and solution are all but identical to that of Sample Problem No. 2 considered in Chapter 3.) The net result, pictured in Fig. 6.8(a), is a build-up of minority carriers in the quasineutral regions immediately adjacent to the edges of the depletion region. The build-up of excess minority carriers adjacent to the depletion region is a consequence of forward biasing, which will prove to be important in subsequent analyses.

Under reverse biasing the depletion region acts like a "sink" for minority carriers, draining the carriers from the adjacent quasineutral regions as pictured in Fig. 6.8(b). A

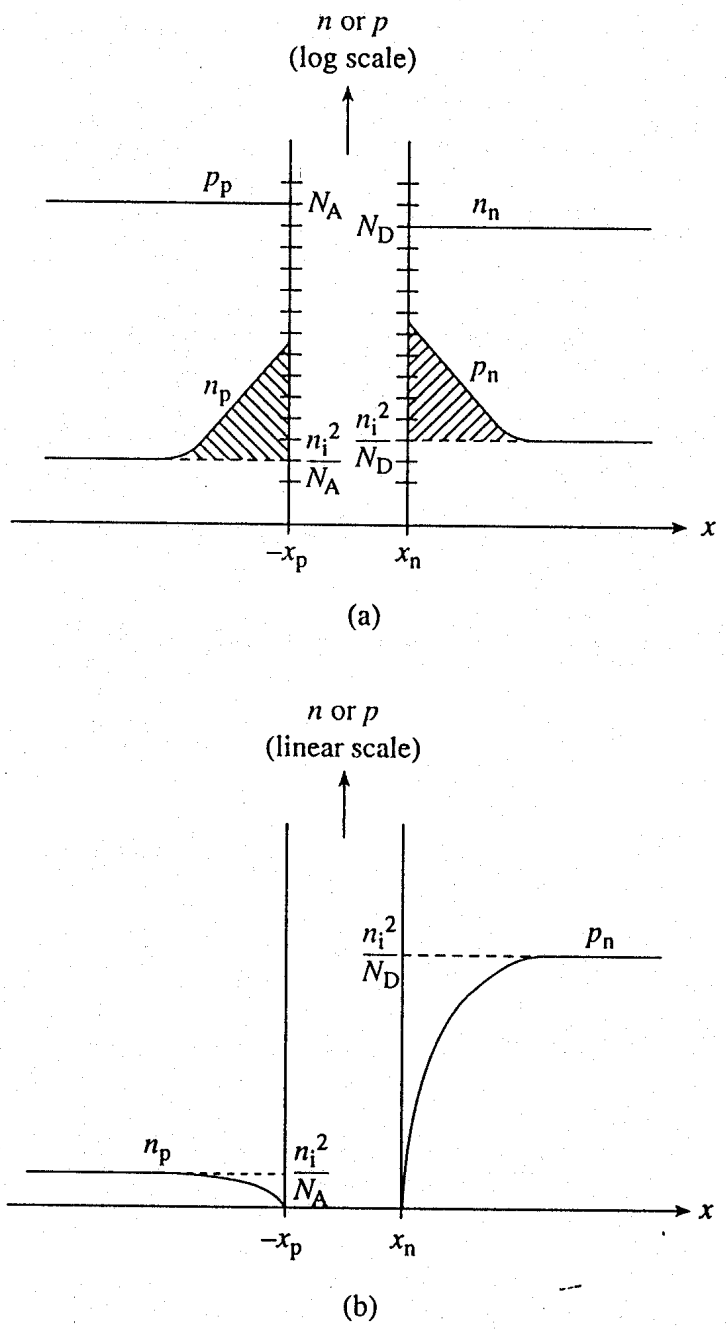

Figure 6.8 Carrier concentrations inside a *pn* junction diode under (a) forward biasing and (b) reverse biasing. The cross-hatching identifies excess minority carriers. Note that (a) is a semilog plot while (b) is a linear plot. $N_A > N_D$ was assumed in constructing the sample plots.

reverse bias of only a few kT/q effectively reduces to zero the minority carrier concentrations at the edges of the depletion region. Larger reverse biases have little effect on the carrier distributions. (This is consistent with the fact that the current, which is directly related to the slope of the carrier distributions at the depletion region edges, saturates for applied biases greater than a few kT/q.) Overall, reverse biasing gives rise to a relatively small deficit of minority carriers in the near vicinity of the depletion region.

Exercise 6.3

P: Figure E6.3 is a dimensioned plot of the steady state carrier concentrations inside a *pn* junction diode maintained at room temperature.

(a) Is the diode forward or reverse biased? Explain how you arrived at your answer.

(b) Do low-level injection conditions prevail in the quasineutral regions of the diode? Explain how you arrived at your answer.

(c) Determine the applied voltage, V_A.

(d) Determine the hole diffusion length, L_P.

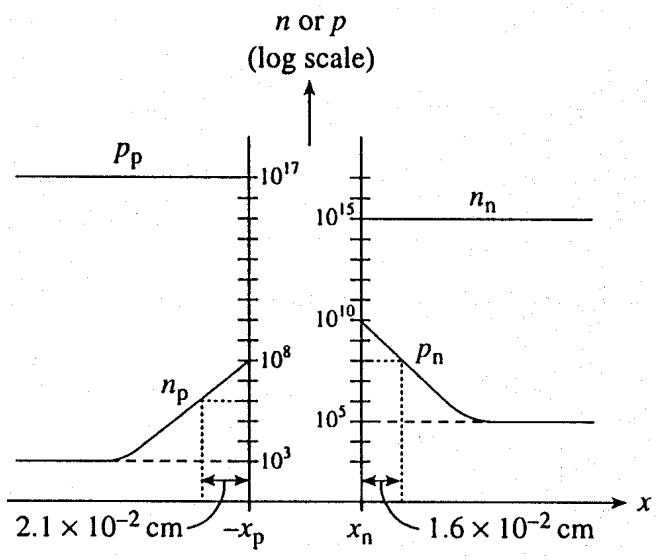

Figure E6.3

S: (a) The diode is forward biased. There is a pile-up or minority carrier excess ($\Delta n_p > 0$ and $\Delta p_n > 0$) at the edges of the depletion region.

(b) Low-level injection conditions *do* prevail. $\Delta p_n \ll n_n$ and $\Delta n_p \ll p_p$ everywhere inside the quasineutral regions.

(c) We can make use of either the depletion edge boundary conditions or the "law of the junction" to determine V_A. Specifically, solving Eq. (6.12) for V_A gives

$$V_A = \frac{kT}{q} \ln\left(\frac{np}{n_i^2}\right) \qquad \ldots -x_p \leq x \leq x_n$$

Evaluating the V_A expression at the n-edge of the depletion region and noting $np \rightarrow n_i^2$ for $x \rightarrow \pm\infty$, we compute

$$V_A = \frac{kT}{q} \ln\left[\frac{n_n(x_n)p_n(x_n)}{n_n(\infty)p_n(\infty)}\right] = (0.0259) \ln\left(\frac{10^{25}}{10^{20}}\right) \cong \mathbf{0.3\ V}$$

(d) Equation (6.23) can be rewritten

$$\Delta p_n(x') = \Delta p_n(x'=0)e^{-x'/L_P}$$

In the near vicinity of the depletion region edge $\Delta p_n \cong p_n$, giving

$$p_n(x') = p_n(0)e^{-x'/L_P}$$

or

$$\ln\left[\frac{p_n(x')}{p_n(0)}\right] = -\frac{x'}{L_P}$$

and

$$L_P = \frac{x'}{\ln\left[\frac{p_n(0)}{p_n(x')}\right]} = \frac{1.6 \times 10^{-2}}{\ln\left(\frac{10^{10}}{10^{8}}\right)} = \mathbf{3.47 \times 10^{-3}\ cm}$$

Exercise 6.4

When reverse biased greater than a few kT/q, the current flowing in a diode is equal to q times the number of minority carriers per second that wander into the depletion region and are swept to the other side of the junction. Under steady state conditions the number of minority carriers thereby extracted per second from the p- and n-sides of the junction must be precisely equal to the number of minority carriers generated per second in the quasineutral regions. In other words, the reverse-bias saturation current may be alternatively viewed as arising from minority carrier generation in the quasineutral regions, with I_0 being equal to q times the number of minority carriers generated per second.

P: Suppose the actual reverse-bias minority carrier distributions in the quasineutral regions are approximated by squared-off distributions as pictured in Fig. E6.4. *All* minority carriers are taken to be depleted a minority carrier diffusion length to either

side of the depletion region. Remembering that low-level injection prevails in the quasineutral regions, and referring to the problem introduction, derive an expression for the reverse-bias saturation current based on the approximate distributions.

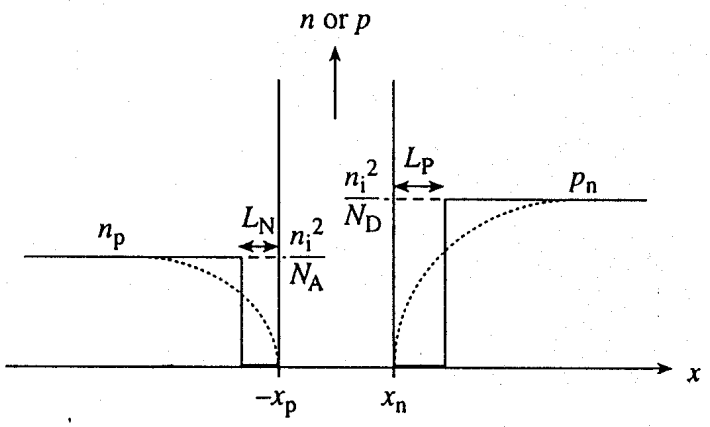

Figure E6.4

S: The carrier generation per second per unit volume based on the approximate distributions is

$$\left.\frac{\partial n}{\partial t}\right|_{\substack{\text{thermal}\\ \text{R–G}}} = -\frac{\Delta n_p}{\tau_n} = \frac{n_i^2/N_A}{\tau_n} \qquad \ldots -L_N - x_p \leq x \leq -x_p$$

and

$$\left.\frac{\partial p}{\partial t}\right|_{\substack{\text{thermal}\\ \text{R–G}}} = -\frac{\Delta p_n}{\tau_p} = \frac{n_i^2/N_D}{\tau_p} \qquad \ldots x_n \leq x \leq x_n + L_P$$

Generation is taking place in volumes of AL_N and AL_P on the p- and n-sides of the junction, respectively. Thus

$$I_0 = q(AL_N)\left(\frac{n_i^2/N_A}{\tau_n}\right) + q(AL_P)\left(\frac{n_i^2/N_D}{\tau_p}\right)$$

$$= qA\left(\frac{D_N}{L_N}\frac{n_i^2}{N_A} + \frac{D_P}{L_P}\frac{n_i^2}{N_D}\right)$$

One obtains the usual I_0 expression!

The approximation introduced in this problem, replacing an exponential distribution with a square distribution extending over one decay length (the same area being enclosed by both distributions), is often a useful analytical tool.

6.2 DEVIATIONS FROM THE IDEAL

A moderately long list of assumptions was involved in deriving the ideal diode equation. Some of the assumptions were made without any a priori justification. It is therefore reasonable to expect that a careful examination of experimental I–V characteristics will reveal discrepancies. Herein we first compare experiment and theory to identify the major deviations from the ideal. Subsequently we treat specific deviations, noting underlying causes and providing required modifications to the ideal theory. Hopefully the reader will not be dismayed by the seemingly band-aid approach in developing an acceptable theoretical description of the diode I–V characteristics. The iterative approach—formulating a simple theory, comparing theory and experiment, revising the theory, comparing the revised theory with experiment, and so on—is common engineering and scientific practice in treating real problems of a complex nature.

6.2.1 Ideal Theory Versus Experiment

The I–V characteristic derived from a Si diode maintained at room temperature and displayed on a 0.1 μA/division linear-scale plot is reproduced in Fig. 6.9. For the most part the characteristic exhibits a form consistent with theoretical expectations. The forward current is a rapidly rising function of the applied voltage, and the reverse current is vanishingly small over a better part of the probed voltage range. However, there is one obvious feature not modeled by the ideal theory: A large reverse-bias current flows when the reverse voltage exceeds a certain value. This phenomenon is referred to as *breakdown.* Although the voltage where breakdown occurs can vary over several orders of magnitude, the phenomenon is common to all *pn* junction diodes. Breakdown constitutes a major deviation from the ideal and is addressed in Subsection 6.2.2.

To determine whether there are additional deviations, it is necessary to take a closer look at the I–V data. A semilog plot of the forward-bias data from the Fig. 6.9 device is displayed in Fig. 6.10(a). Reverse-bias data from the device are replotted in Fig. 6.10(b) employing an expanded current scale of 50 pA/division. Data for both plots were obtained using a HP4145B Semiconductor Parameter Analyzer. The noticeable fluctuations in the extremely small reverse bias current are caused by noise inherent in the device and measurement system.

Examining the Fig. 6.10(a) forward-bias data, we note that the curve exhibits the expected q/kT slope for applied voltages between approximately 0.35 V and 0.7 V. However, there are obvious deviations outside the cited voltage range. At forward biases in excess of 0.7 V the slope progressively decreases or the characteristic "slopes over." This deviation, more or less to be expected, is related to the high level of current flowing in the device when $V_A \rightarrow V_{bi}$ and is treated in Subsection 6.2.4.

For voltages below 0.35 V the current levels are quite small and the deviation is clearly of a different origin. In addition, the observed current is far in excess of the expected value and the slope of the characteristic curiously approaches $q/2kT$. These facts suggest we may be observing a current component either overlooked or neglected in the derivation of the ideal diode equation. This suspicion is further enhanced by an examination of the reverse bias data. For one, the device has an estimated $I_0 \cong 10^{-14}$A, some three orders of magni-

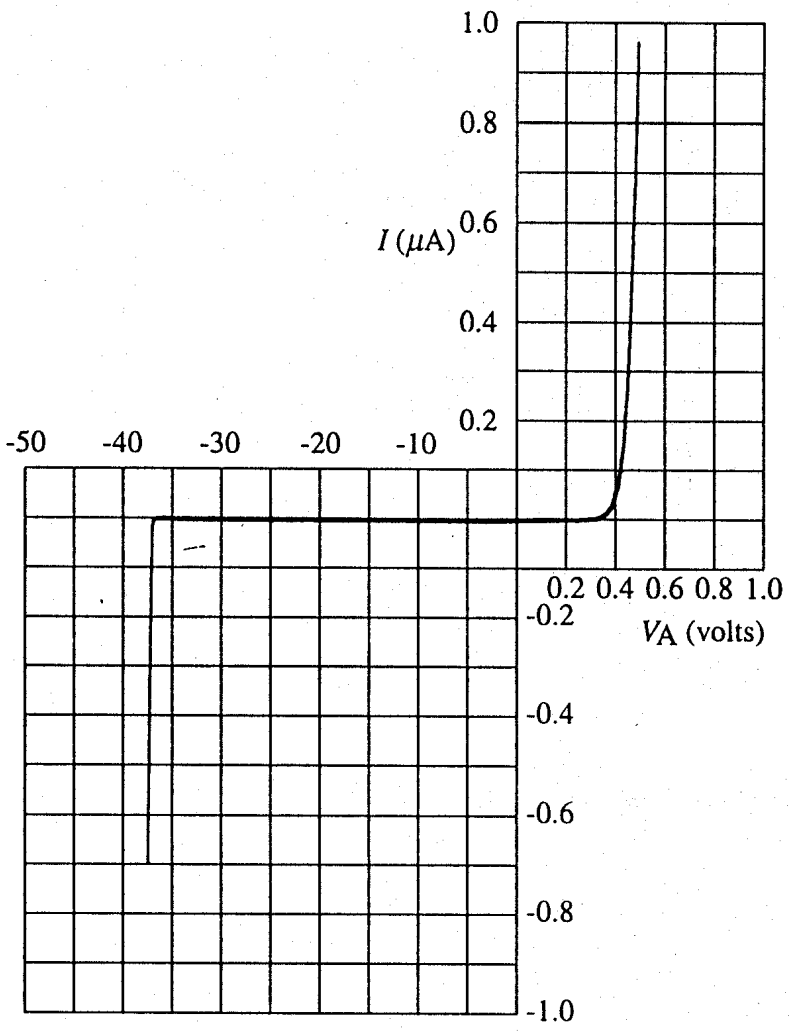

Figure 6.9 Linear plot of the measured *I–V* characteristic derived from a commercially available Si *pn* junction diode maintained at room temperature. The plot permits a coarse evaluation of the diode characteristic. Note the change in voltage scale in going from forward to reverse bias.

tude smaller than the reverse current observed at $V_A = -5V$! Moreover, the Fig. 6.10(b) characteristic does not saturate as predicted by the ideal theory. Rather, the current continually increases with increasing reverse bias. As will be verified in Subsection 6.2.3, the cited reverse-bias and small forward-bias deviations are caused by the added current arising from carrier recombination–generation in the depletion region. Carrier R–G was assumed to be negligible throughout the depletion region in deriving the ideal diode equation.

Although feature details do vary from device to device, and other nonidealities may be encountered, the data displayed in Figs. 6.9 and 6.10 are fairly representative of the *I–V* characteristics derived from commercially available Si *pn* junction diodes maintained at room temperature. Similar characteristics are exhibited by GaAs diodes. Ge diodes maintained at room temperature and Si diodes operated at elevated temperatures, on the other hand, are often found to more closely approach the ideal, specifically exhibiting saturating reverse-bias characteristics. An explanation of this difference in behavior is included in the R–G current discussion.

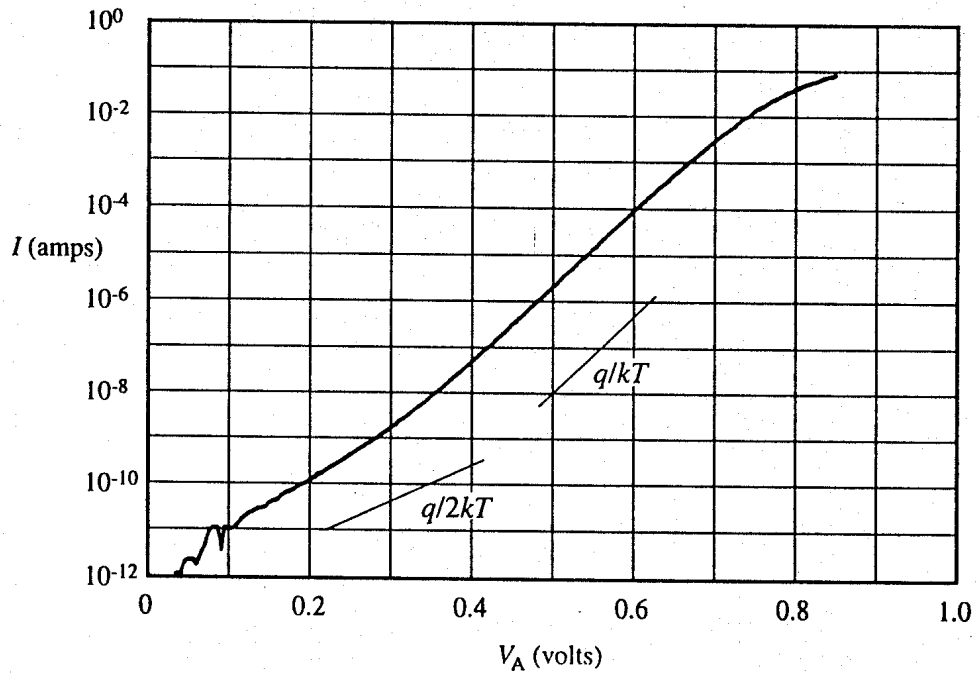

(a)

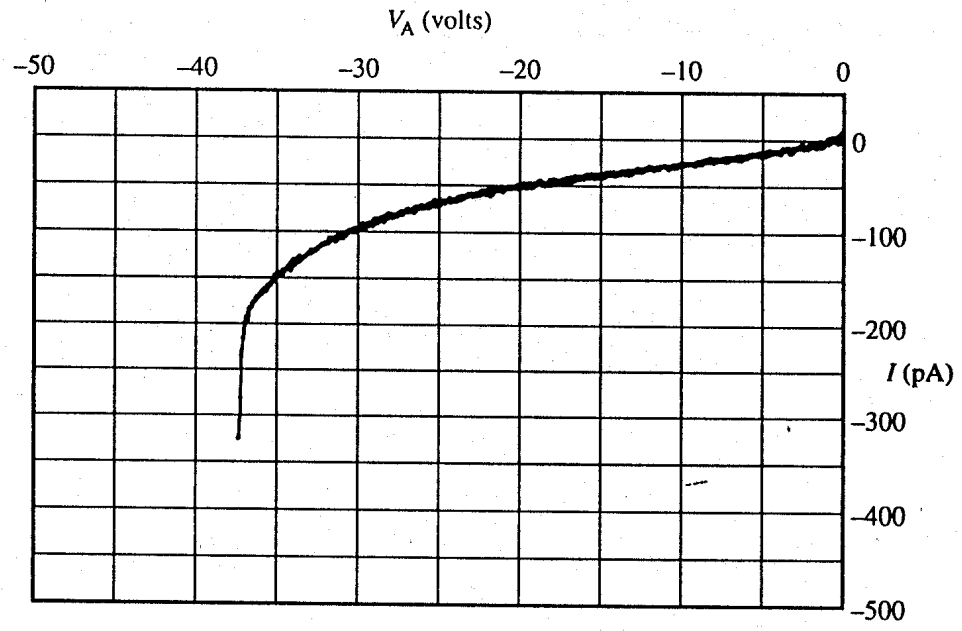

(b)

Figure 6.10 Detailed plots of the measured I–V characteristic derived from a commercially available Si *pn* junction diode maintained at room temperature. The Fig. 6.9 and Fig. 6.10 characteristics are from the same device. (a) Semilog plot of the forward-bias current versus voltage. (b) Expanded scale plot of the reverse-bias current versus voltage.

6.2.2 Reverse-Bias Breakdown

Although referred to as "breakdown," the large reverse current that flows when the reverse voltage exceeds a certain value is a completely reversible process. That is, breakdown does not damage the diode in any way. The current must be limited, of course, to avoid excessive heating. The absolute value of the reverse voltage where the current goes off to infinity is known as the breakdown voltage and is given the symbol V_{BR}. Practical V_{BR} measurements typically quote the voltage where the current exceeds a preselected value such as 1 μA or 1 mA. The expected breakdown voltage of planar (one-dimensional) p^+-n and n^+-p step-junction diodes as a function of the nondegenerate-side doping is plotted in Fig. 6.11 for select semiconductors. At a given doping, V_{BR} tends to increase with the band gap of the semiconductor used to fabricate the diode. Of greater significance, the doping on the lightly doped side of the junction can be used to vary V_{BR} from a few volts to over a thousand volts. Note that the doping dependence above the dashed line in Fig. 6.11 is roughly described by

$$V_{BR} \propto \frac{1}{N_B^{0.75}} \tag{6.33}$$

where N_B is the doping on the lightly doped side of the junction.

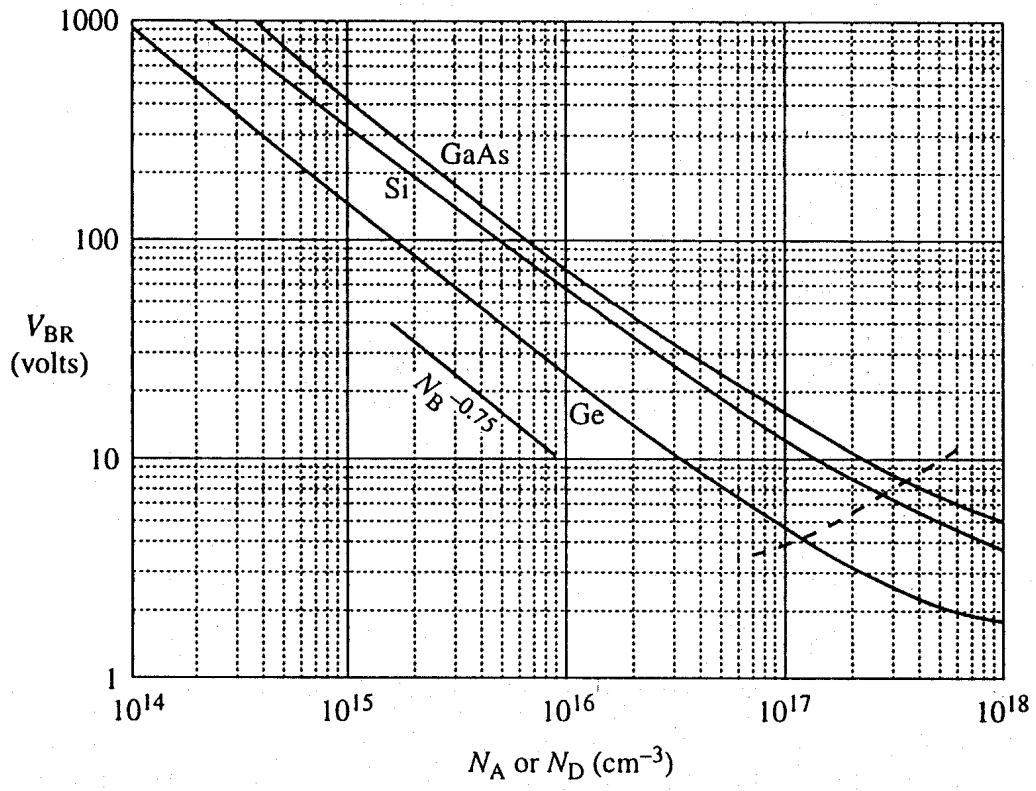

Figure 6.11 Breakdown voltage as a function of the nondegenerate-side doping in planar p^+-n and n^+-p step-junction Ge, Si, and GaAs diodes. Avalanche is the dominant breakdown process for dopings above the dashed line. T = 300 K. (After Sze[1], © 1981 by John Wiley & Sons, Inc. Reprinted with permission.)

From a theoretical standpoint, breakdown is directly related to the failure of the "no other processes" assumption in the derivation of the ideal diode equation. In fact, two "other processes"—avalanching and the Zener process—can cause the breakdown current. Avalanching is typically the dominant process, with the Zener process only becoming important when both sides of the junction are heavily doped. In what follows, we delve into the physical nature of the two processes and provide process-specific information.

Avalanching

Working up to a physical description of the avalanching phenomenon, let us first consider a reverse-biased diode where V_A is relatively small and far below the breakdown voltage. Ideally, the reverse current flowing in the diode is due to minority carriers randomly entering the depletion region and being accelerated by the electric field in the region to the other side of the junction. In crossing the depletion region the carrier acceleration is not continuous but is interrupted by energy-losing collisions with the semiconductor lattice, as envisioned in Fig. 6.12(a). Since the mean free path between collisions is $\sim 10^{-6}$ cm, and a median depletion width is $\sim 10^{-4}$ cm, a carrier can undergo tens to thousands of collisions in crossing the depletion region. Thus at small applied reverse biases the energy lost by the carriers per collision is relatively small. The energy transferred to the lattice simply causes lattice vibrations—there is just localized heating that is readily dissipated.

With increasing reverse bias the amount of energy transferred to the semiconductor lattice per collision systematically increases. Approaching the breakdown voltage, the energy transferred per collision becomes sufficient to ionize a semiconductor atom. By "ionize" we mean the collision frees a valence electron from the atom, or causes an electron from the valence band to jump into the conduction band, thereby creating an electron-hole pair. This phenomenon, called *impact ionization,* was previously visualized in Fig. 3.15(f). The added carriers created by impact ionization are immediately accelerated by the electric field in the depletion region. Consequently, they and the original carriers make additional collisions and create even more carriers as envisioned in Fig. 6.12(b). The result is a snowballing creation of carriers very similar to an avalanche of snow on a mountain side. At the breakdown voltage the carrier creation and reverse current effectively go off to infinity.

A couple of clarifying comments are in order concerning the preceding discussion and avalanching. For one, the Fig. 6.12(b) energy band diagram is not, and realistically could not be, drawn to scale. If the breakdown voltage were 100 V, for example, the distance between the *p*- and *n*-side Fermi levels would have to be approximately 100 times the E_c minus E_v band gap distance. Second, it is important to note that avalanche breakdown does not occur sharply at $V_A = -V_{BR}$. When the reverse-bias characteristics are examined carefully as in Fig. 6.10(b), they are found to exhibit a sloping approach to breakdown. There is considerable carrier multiplication a few volts before reaching breakdown and even some carrier multiplication at voltages far below breakdown. The reason is that the distance between collisions is a random variable statistically distributed about the mean value. Thus carriers can occasionally gain sufficient energy to have an ionizing collision at voltages far below breakdown. At a few volts below breakdown the

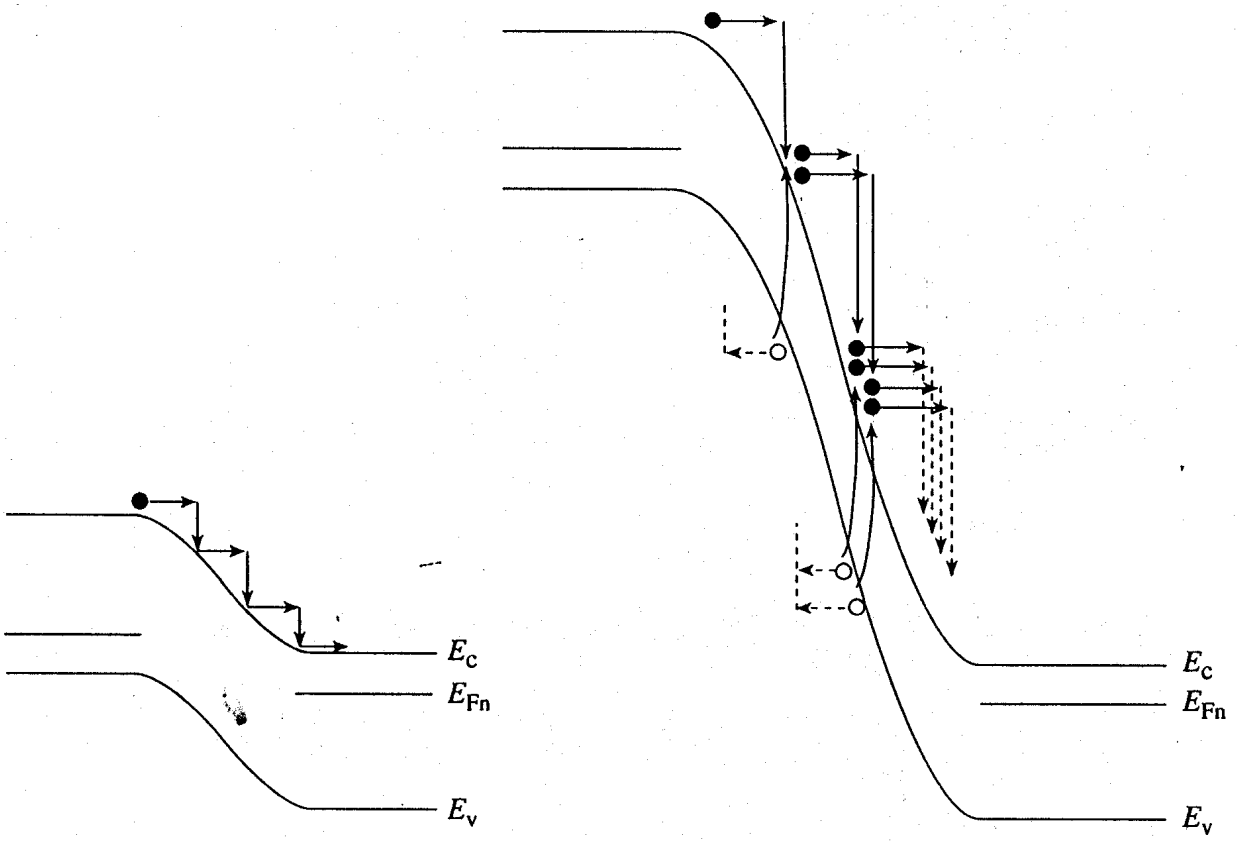

(a) Small reverse bias (b) $|V_A| \rightarrow V_{BR}$

Figure 6.12 Carrier activity inside the depletion region of a reverse-biased *pn* junction diode when (a) $|V_A| \ll V_{BR}$ and (b) $|V_A| \rightarrow V_{BR}$. Carrier multiplication due to impact ionization and the resultant avalanche is pictured in (b).

number of carriers gaining sufficient energy to have an ionizing collision becomes quite large. The increase in current associated with the carrier multiplication is modeled by introducing a *multiplication factor, M.* If I_0 is taken to be the current without any carrier multiplication, then

$$M \equiv \frac{|I|}{I_0} \tag{6.34}$$

An empirical fit to experimental data gives

$$M = \frac{1}{1 - \left[\dfrac{|V_A|}{V_{BR}}\right]^m} \tag{6.35}$$

where m takes on a value between 3 and 6, depending on the semiconductor used to fabricate the diode. Please note that the multiplication factor can be used to correct the ideal diode equation to account for carrier multiplication and avalanching.

We next seek to explain the V_{BR} dependence noted in the breakdown introduction. From the qualitative description of avalanching, it was concluded that breakdown occurs when the carriers gain an ionizing amount of energy in traveling a lattice-scattering mean free path. This should be true independent of the junction doping. A specific energy gain over a given distance, however, corresponds to a specific electric field. In other words, breakdown occurs when the electric field in the depletion region reaches some critical value, $\mathscr{E}_{CR}$, essentially independent of the junction doping.

Considering a step junction, employing Eqs. (5.35) and (5.37), and evaluating the electric field at $x = 0$, we find

$$\mathscr{E}(0) = -\frac{qN_D}{K_S\varepsilon_0}x_n = -\left[\frac{2q}{K_S\varepsilon_0}\left(\frac{N_AN_D}{N_A + N_D}\right)(V_{bi} - V_A)\right]^{1/2} \tag{6.36}$$

Next, squaring the preceding expression and making use of the fact that $\mathscr{E}(0) \rightarrow \mathscr{E}_{CR}$ when $V_{bi} - V_A \rightarrow V_{bi} + V_{BR} \cong V_{BR}$, we obtain

$$\mathscr{E}_{CR}^2 = \frac{2q}{K_S\varepsilon_0}\left(\frac{N_AN_D}{N_A + N_D}\right)V_{BR} \tag{6.37}$$

Since $\mathscr{E}_{CR}$ is independent of doping, the right-hand side of Eq. (6.37) must likewise be independent of doping. The right-hand side of Eq. (6.37) will be independent of doping if

$$V_{BR} \propto \frac{N_A + N_D}{N_AN_D} \tag{6.38}$$

or for asymmetrically doped junctions

$$V_{BR} \propto \frac{1}{N_B} \tag{6.39}$$

The Eq. (6.39) result is not precisely as observed experimentally, but it is acceptably close given the simplicity of the argument.

Concerning the V_{BR} band gap (or semiconductor) dependence, we again note that breakdown occurs when the carriers gain an ionizing amount of energy in traveling a lattice-scattering mean free path. The required ionization energy obviously increases with increasing E_G, but the mean free path is found to vary only slightly for the semiconductors cited in Fig. 6.11. Thus, consistent with Fig. 6.11, the breakdown voltage is expected to progressively increase in going from Ge to Si to GaAs.

One more dependence is worth mentioning. The V_{BR} due to avalanching is found to increase as the temperature goes up. As noted in the mobility discussion in Subsection 3.1.3, lattice scattering increases as the temperature increases. Increasing lattice scat-

tering means a smaller mean free path, a larger critical electric field for avalanching, and hence a higher breakdown voltage.

Finally, the discussion has focused on planar step-junction diodes. Separate breakdown curves apply to linearly graded diodes. Moreover, step-junction diodes formed by diffusion or ion-implantation through a mask always have curved, nonplanar lateral edges. For a given applied voltage the electric field is greater in the nonplanar region than in the planar part of the device. Hence breakdown occurs sooner in the nonplanar regions, lowering the V_{BR} of the diode. This "curvature" effect becomes more pronounced as the depth of the junction decreases. Special edge modifications have been developed to minimize the effect.

(C) Exercise 6.5

P: Compute and make a plot of the multiplication factor (M) versus $|V_A|/V_{BR}$ when $m = 3$ and $m = 6$. Orient the axes so a reverse-current-like plot is obtained; i.e., plot M increasing downward and $|V_A|/V_{BR}$ increasing to the left. Discuss the plotted results.

S: The computer program script and resultant plot (Fig. E6.5) follow. Using MATLAB, the author was only able to obtain the desired axes orientation by plotting $-M$ versus $-|V_A|/V_{BR}$. The plot is noted to be quite similar to the left-hand side of Fig. 6.10(b). A perhaps surprising $2\times$ increase in current is predicted for applied voltages less than 80% and 90% of the way to V_{BR} for $m = 3$ and $m = 6$, respectively. There is already a carrier enhancement of ~10% ($M = 1.1$) at $0.45V_{BR}$ when $m = 3$ and at $0.65V_{BR}$ when $m = 6$.

MATLAB program script...

```
%Exercise 6.5...Multiplication factor

%Initialization
close
clear

%M calculation
x=linspace(0,.99);      %x=|VA|/VBR
M3=1 ./(1-x.^3);        %M when m=3
M6=1 ./(1-x.^6);        %M when m=6

%Plotting result
plot(-x,-M3,-x,-M6); grid
axis([-1 0 -10 0])
xlabel('-|VA|/VBR')
ylabel('-Multiplication factor')
text(-0.8,-2.5,'m = 3')
text(-0.95,-1.5,'m = 6')
```

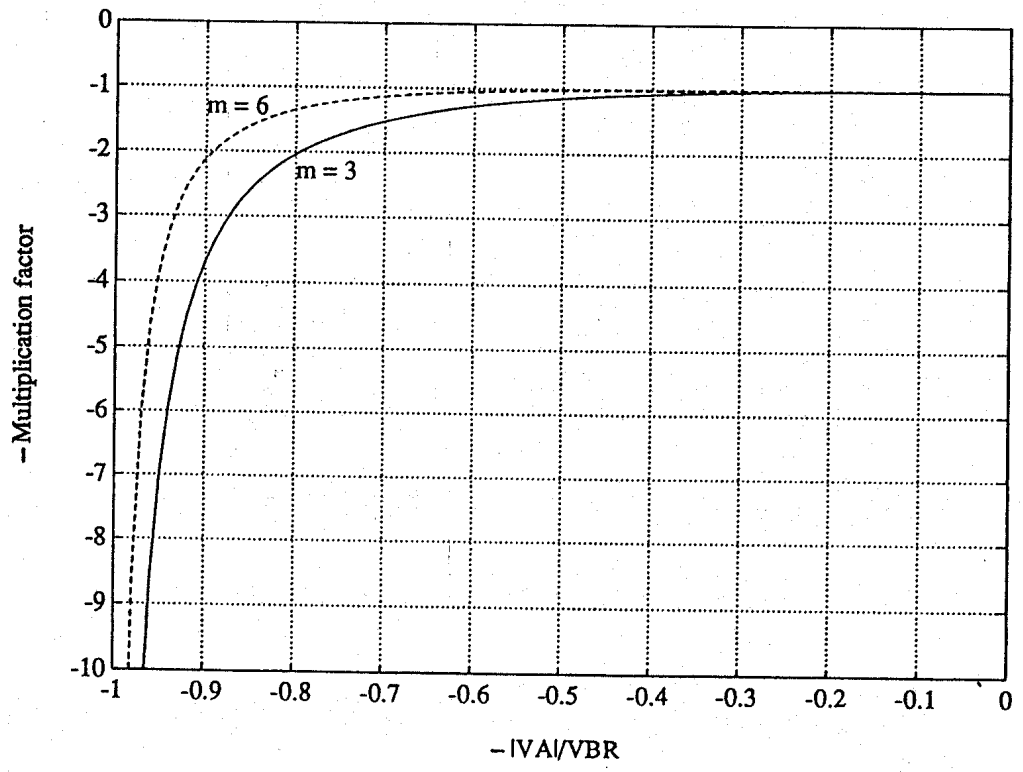

Figure E6.5

Zener Process

Zener process is the name given to the occurrence of "tunneling" in a reverse-biased diode. *Tunneling* is the first phenomenon we have encountered that is of a purely quantum-mechanical nature. It has no classical analog. The general nature and basic features of tunneling can be understood with the aid of Fig. 6.13. The particle pictured in the figure is taken to be positioned on the left-hand side of a potential energy barrier. The height of the barrier is assumed to be greater than the kinetic energy of the particle. Classically, the only way a particle such as an electron could move to the other side of the barrier would be to gain additional energy and go over the top of the barrier. Quantum mechanically, there is another way the particle can get to the other side of the barrier: It can go through the barrier. Tunneling is going "through" a potential energy barrier. It should be emphasized that the particle energy remains constant during the process. Also (thinking classically) the particle and the barrier are not damaged in any way.

There are two major requirements for tunneling to occur and be significant:

(1) There must be filled states on one side of the barrier and empty states on the other side of the barrier at the same energy. Tunneling cannot take place into a region void of allowed states.

(2) The width of the potential energy barrier, d in Fig. 6.13, must be very thin. Quantum-mechanical tunneling becomes significant only if $d < 100$ Å $= 10^{-6}$ cm.

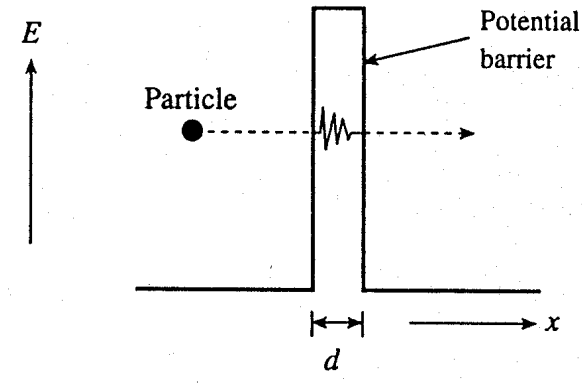

Figure 6.13 General visualization of tunneling.

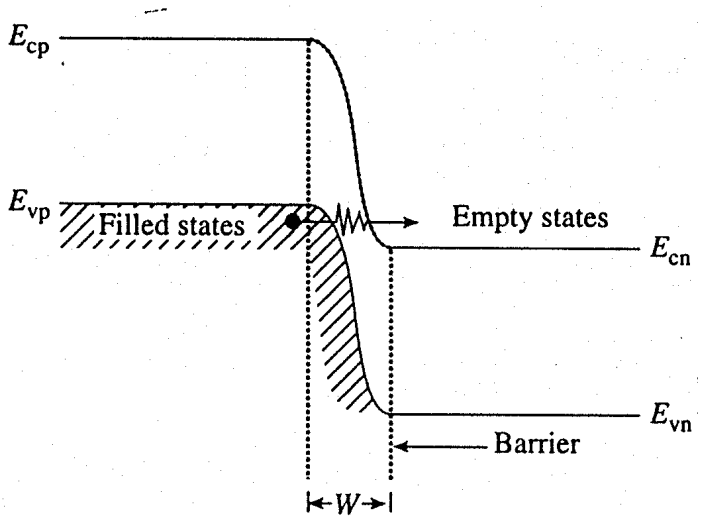

Figure 6.14 Visualization of tunneling in a reverse-biased *pn* junction diode.

Visualization of the Zener process, tunneling in a reverse-biased *pn* junction diode, is presented in Fig. 6.14. The particles doing the tunneling are valence band electrons on the *p*-side of the junction. The potential energy barrier classically restricting these electrons to the *p*-side of the junction is outlined in the figure. Tunneling takes place when the electrons pass through the barrier to empty states at the same energy in the conduction band on the *n*-side of the junction. The greater the reverse bias, the larger the number of filled valence-electron states on the *p*-side placed opposite empty conduction-band states on the *n*-side, and hence the greater the reverse-bias tunneling current.

For tunneling to be significant, the barrier thickness, roughly the depletion width in the case of the *pn* junction diode, must be $<10^{-6}$ cm. Referring to Fig. E5.3, we find Si diode depletion widths $<10^{-6}$ cm necessitate dopings in excess of $10^{17}/\text{cm}^3$ on the "lightly" doped side of the junction. Thus the Zener process is important only in diodes that are heavily doped on both sides of the junction. The breakdown voltage of the diodes is correspondingly small. The Zener process makes a significant contribution to the break-

down current in diodes where $V_{BR} < 6E_G/q$ (~6.7 V in Si at 300 K) and dominates in diodes where $V_{BR} < 4E_G/q$ (~4.5 V in Si at 300 K).

Two experimental observations can be used to distinguish between avalanching and Zener process breakdown. First, whereas the V_{BR} associated with avalanching increases with increasing T, V_{BR} *decreases* with increasing T if the Zener process is dominant. Second, the breakdown characteristics associated with the Zener process are very "soft." The current exhibits a very slow approach to infinity even when observed on a relatively coarse scale.

Historically, the Zener process was the first proposed to explain reverse-bias breakdown. All diodes specifically fabricated to make use of the breakdown characteristic came to be known as Zener diodes. The name continues to be applied to all diodes making use of the breakdown characteristic, even though those with breakdown voltages in excess of $6E_G/q$ are functionally avalanche diodes.

6.2.3 The R–G Current

In comparing theory and experiment, a current far in excess of that predicted by the ideal diode theory was found to exist at small forward biases and all reverse biases in Si diodes maintained at room temperature. The observed "extra" current arises from thermal carrier recombination–generation in the depletion region that was assumed to be negligible in the derivation of the ideal diode equation. How thermal R–G in the depletion region gives rise to an added current component can be understood with the aid of Fig. 6.15. First consider the reverse-bias case modeled in Fig. 6.15(a). Heretofore in all quantitative analyses, and even in the qualitative derivation of the ideal diode equation, we associated the reverse current with the minority carriers wandering into the depletion region from the two sides of the junction. When the diode is reverse biased, however, the carrier concentrations in the depletion region are reduced below their equilibrium values, leading to the thermal generation of electrons and holes throughout the region.† The large electric field in the depletion region rapidly sweeps the generated carriers into the quasineutral regions, thereby adding to the reverse current. Forward biasing increases the carrier concentrations in the depletion region above their equilibrium values giving rise to carrier recombination in the region. As envisioned in Fig. 6.15(b), one can effectively view the resulting added forward current as arising from the carriers that cannot make it over the potential hill being partially eliminated via recombination at R–G centers in the depletion region.

Seeking to establish a quantitative expression for the added current, I_{R-G}, arising from thermal recombination–generation in the depletion region, we note that the net R–G rate is the same for electrons and holes under steady state conditions. Moreover, for every electron-hole *pair* created or destroyed in the depletion region per second, *one* electron per second flows into or out of the diode contacts. Summing either the electrons or the holes created/destroyed throughout the depletion region per second and multiplying by q should

† Use of the term *depletion region* in the present context sometimes leads to confusion. It must be remembered that the carrier concentrations in the depletion region are not zero or automatically less than their equilibrium values, but are merely small compared to the background doping concentrations.

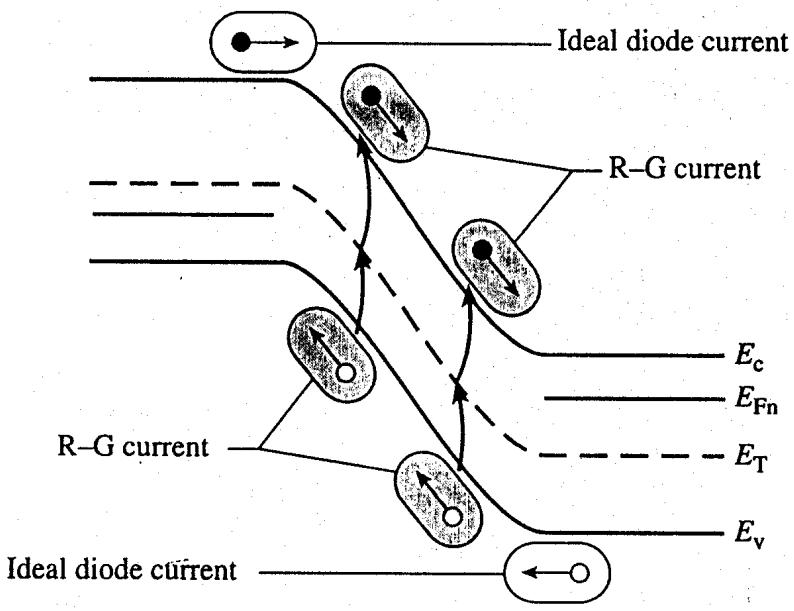

(a) Reverse bias

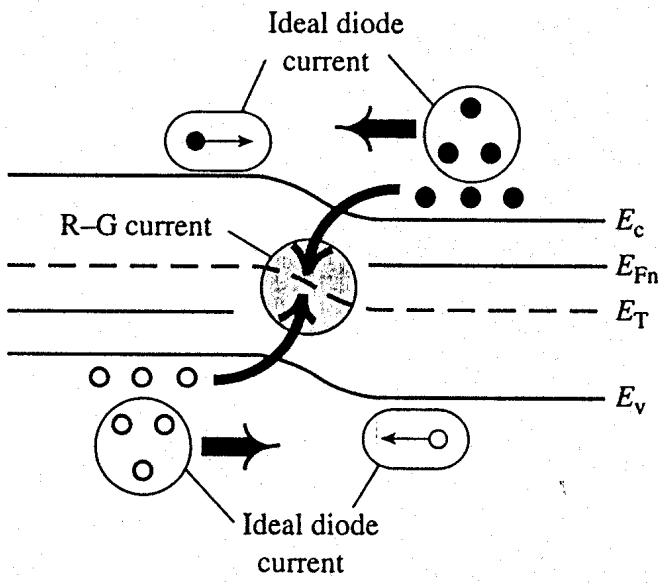

(b) Forward bias

Figure 6.15 The R–G current. Visualization of the additional current resulting from (a) reverse-bias generation and (b) forward-bias recombination in the depletion region.

therefore give the magnitude of the added current flowing in the device. Proceeding as indicated and accounting for the polarity of the current yields

$$I_{R\text{-}G} = -qA \int_{-x_p}^{x_n} \left. \frac{\partial n}{\partial t} \right|_{\substack{\text{thermal} \\ R\text{-}G}} dx \tag{6.40}$$

Note that, because of the conditions prevalent in the depletion region, the familiar special-case R–G relationship, $\partial n/\partial t|_{\text{thermal R–G}} = -\Delta n/\tau_n$, is not applicable. Rather, the general-case result initially presented as Eq. (3.35) must be employed:

$$\left.\frac{\partial n}{\partial t}\right|_{\substack{\text{thermal}\\ \text{R–G}}} = -\frac{np - n_i^2}{\tau_p(n + n_1) + \tau_n(p + p_1)} \tag{6.41}$$

and

$$I_{\text{R–G}} = qA\int_{-x_p}^{x_n} \frac{np - n_i^2}{\tau_p(n + n_1) + \tau_n(p + p_1)}\,dx \tag{6.42}$$

For reverse biases greater than a few kT/q, the carrier concentrations become quite small throughout most of the depletion region. With the carrier concentrations being negligible ($n \to 0$, $p \to 0$), the integral in Eq. (6.42) is readily evaluated to obtain

$$\boxed{I_{\text{R–G}} = -\frac{qAn_i}{2\tau_0}W} \quad \ldots \text{ reverse biases} > \text{few } kT/q \tag{6.43}$$

where

$$\tau_0 \equiv \frac{1}{2}\left(\tau_p\frac{n_1}{n_i} + \tau_n\frac{p_1}{n_i}\right) = \frac{1}{2}\left(\tau_p e^{(E_T - E_i)/kT} + \tau_n e^{(E_i - E_T)/kT}\right) \tag{6.44}$$

For forward biases the carrier concentrations cannot be neglected and even an approximate evaluation of the Eq. (6.42) integral becomes rather involved. We merely note that $I_{\text{R–G}}$ is expected to vary roughly as $\exp(qV_A/\eta kT)$, $1 < \eta \leq 2$, for forward biases greater than a few kT/q.[2] Typically, the expected η is close to 2, and the combined forward and reverse bias dependence is approximately described by

$$\boxed{I_{\text{R–G}} = \frac{qAn_i}{2\tau_0}W\frac{(e^{qV_A/kT} - 1)}{\left(1 + \dfrac{V_{bi} - V_A}{kT/q}\dfrac{\sqrt{\tau_n\tau_p}}{2\tau_0}e^{qV_A/2kT}\right)}} \tag{6.45}$$

With the introduction of a second current component, it is common practice to refer to the current described by the ideal diode equation as the *diffusion current*, I_{DIFF}. The diffusion current expression is rewritten here to facilitate a comparison of the two

components:

$$I_{\text{DIFF}} = qA\left(\frac{D_N}{L_N}\frac{n_i^2}{N_A} + \frac{D_P}{L_P}\frac{n_i^2}{N_D}\right)(e^{qV_A/kT} - 1) \tag{6.46}$$

The total current flowing in the diode is of course just the sum of the diffusion current and the R–G current:

$$I = I_{\text{DIFF}} + I_{\text{R-G}} \tag{6.47}$$

We are now in a position to explain earlier experimental observations. In Si diodes at room temperature $qAn_iW/2\tau_0 \gg I_0$ and the $I_{\text{R-G}}$ current dominates at reverse biases and small forward biases. Since the reverse bias $I_{\text{R-G}}$ is proportional to W, the reverse current never saturates, but continually increases with increasing reverse bias. The forward bias $I_{\text{R-G}}$ varies as $\exp(qV_A/2kT)$ for $V_A >$ few kT/q, consistent with experimental observations at small forward biases. With increasing forward biases the I_{DIFF} component, which increases more rapidly with voltage, eventually overtakes the $I_{\text{R-G}}$ component, leading to the q/kT region on a semilog plot of the forward-bias characteristics. Because $I_{\text{DIFF}} \propto n_i^2$ while $I_{\text{R-G}} \propto n_i$, the relative weight of the two components varies significantly from semiconductor to semiconductor. Whereas $qAn_iW/2\tau_0 \gg I_0$ in Si and GaAs diodes at room temperature, the larger n_i of Ge typically makes $I_0 > qAn_iW/2\tau_0$ in Ge diodes at room temperature. Also, since $I_0 \propto n_i^2$ while the reverse bias $I_{\text{R-G}} \propto n_i$, the reverse bias diffusion component of the current will increase at a faster rate with increasing temperature. The diffusion component eventually dominates at a sufficiently elevated temperature. The n_i dependence explains the experimental observations that Ge diodes maintained at room temperature and Si diodes operated at elevated temperatures are often found to more closely approach the ideal, specifically exhibiting saturating reverse-bias characteristics.

(C) Exercise 6.6

If the weak voltage dependence of the factors multiplying the exponential in the $I_{\text{R-G}}$ expression is ignored, the total *pn* junction diode current for forward biases greater than a few kT/q may be approximately modeled by

$$I = \underset{\uparrow}{I_{01}}e^{qV_A/kT} + \underset{\uparrow}{I_{02}}e^{qV_A/2kT}$$
$$I_{\text{DIFF}} \qquad I_{\text{R-G}}$$

where *both* I_{01} and I_{02} are taken to be constants independent of voltage.

P: (a) Compute I_{01} and I_{02} for a Si p^+-n step junction diode maintained at 300 K with $A = 10^{-4}$ cm^2, $N_D = 10^{16}$/cm^3, and $\tau_n = \tau_p = \tau_0 = 10^{-6}$ sec. In the I_{02} computation, assume that the $\exp(qV_A/2kT)$ term in the denominator of the I_{R-G} expression is much greater than unity and set $V_A = V_{bi}/4$ in evaluating voltage-dependent terms. As in previous exercises compute V_{bi} using $V_{bi} = (E_G/2q) + (kT/q)\ln(N_D/n_i)$.

(b) Repeat part (a) for a Ge p^+-n step junction diode maintained at 300 K. Assume a set of parameters identical to the part (a) Si diode except that $\mu_p = 1500$ cm^2/V-sec, $n_i = 2.5 \times 10^{13}$/cm^3, and $K_S = 16$.

(c) Making use of the simplified current relationship introduced in this problem, construct a semilog plot of I versus V_A that simultaneously displays the forward-bias characteristics of the previously described Si and Ge diodes. Limit the plot axes to $0\text{ V} \leq V_A \leq 1\text{ V}$ and $10^{-12}\text{ A} \leq I \leq 10^{-3}\text{ A}$. Begin the calculation at $V_A = 0.1$V. Discuss your results.

S: The computed I_{01} and I_{02} values for the two diodes are summarized in the table presented below. The part (c) computer program and plot follow the table. The I_{01} and I_{02} values are stored in memory after running the listed computer program and were accessed from the MATLAB *Command* window.

As expected, $I_{02} \gg I_{01}$ for the Si diode while $I_{01} > I_{02}$ for the Ge diode. Because of the small band gap and corresponding large n_i, large forward currents flow in the Ge diode at relatively small voltages, making it all but impossible to observe the I_{R-G} component. Conversely, both the I_{DIFF} and I_{R-G} components are clearly evident on the silicon diode plot.

	Silicon	*Germanium*
I_{01}	5.38×10^{-16} A	6.23×10^{-9} A
I_{02}	2.08×10^{-13} A	8.34×10^{-10} A

MATLAB program script...

```
% Comparison of forward bias I-VA for Si and Ge diodes at 300K.
%   This program uses a simplified formula for the current:
%   I = I01*exp(qVA/(kT)) + I02*exp(qVA/(2kT)).
%   Also, Vbi=EG/2q+(kT/q)ln(ND/ni).
```

```
%Initialization
close
clear

% Constants
T=300;                  % Temperature in Kelvin
k=8.617e-5;             % Boltzmann constant eV/K
e0=8.85e-14;            % permittivity of free space (F/cm)
q=1.602e-19;            % charge on an electron (coul)
KS=[11.8 16];           % Dielectric constant [Si Ge]
ni=[1.0e10 2.5e13];     % intrinsic carrier conc. at 300K [Si Ge]
μp=[437 1500];          % hole mobility [Si Ge]
EG=[1.12 0.66];         % band gap [Si Ge]

% Given Constants
A=1.0e-4;       % cm^2
ND=1.0e16;      % cm^(-3)
taun=1.0e-6;    % seconds
taup=1.0e-6;    % seconds

% I01
DP=k*T.*μp;
LP=sqrt(DP.*taup);
I01=q*A.*(DP./LP.*ni.^2./ND);

% I02
Vbi=EG/2+k*T.*log(ND./ni);
W=sqrt(2.*KS*e0/(q*ND).*Vbi);
I02=q*A.*ni/sqrt(taun*taup).*W.*(k*T)./(3 .*Vbi./4);

% Currents for both Silicon (ISi) and Germanium (IGe)
VA=linspace(0.1,1);
ISi=I01(1).*exp(VA./(k*T))+I02(1).*exp(VA./(2*k*T));
IGe=I01(2).*exp(VA./(k*T))+I02(2).*exp(VA./(2*k*T));

% Plot
semilogy(VA,ISi,VA,IGe,'-'); grid
axis([0 1 1.0e-12 1.0e-3]);
xlabel('VA(volts)');
ylabel('I(A)');
text(.7, 1.4e-9,'T = 300K');
text(.7, 4.0e-10,'ND = 1.0e16 /cm^3');
text(.25, 1.4e-5,'Ge');
text(.48, 1.4e-8,'Si');
```

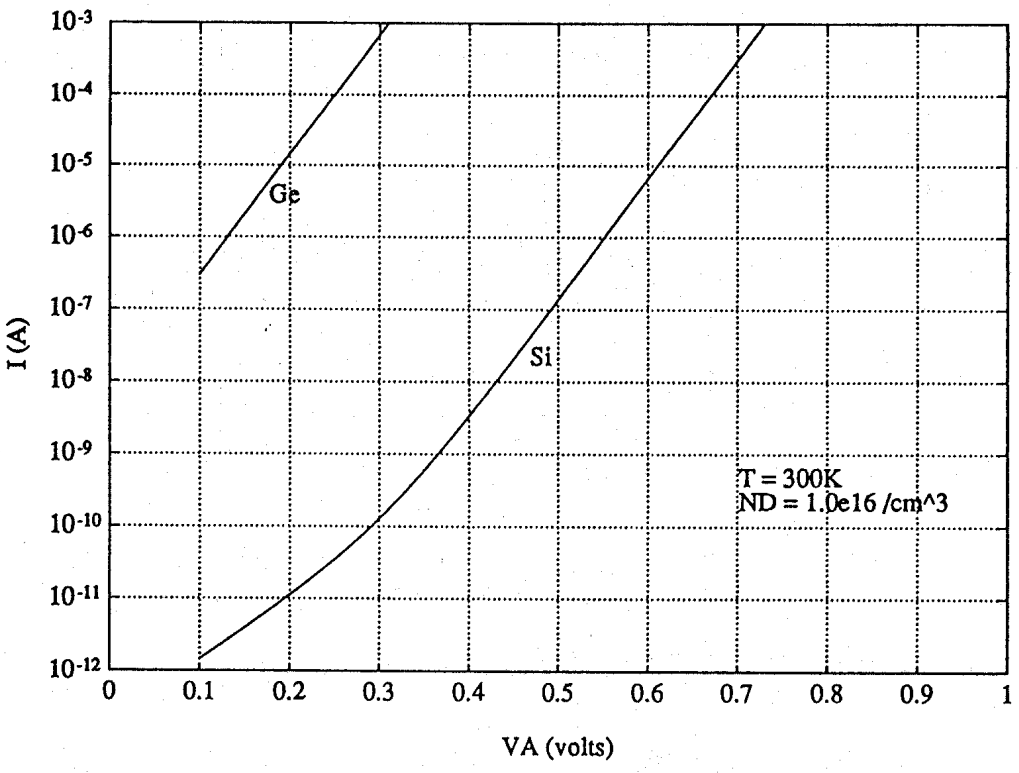

Figure E6.6

Exercise 6.7

A generalization of the forward-bias modeling expression in Exercise 6.6 is commonly introduced in analyzing experimental data. Specifically, one employs

$$I = \underset{\uparrow}{I_{01}e^{qV_A/n_1kT}} + \underset{\uparrow}{I_{02}e^{qV_A/n_2kT}}$$
$$I_{DIFF} \qquad\qquad I_{R-G}$$

where n_1 and n_2 are arbitrary constants determined by a match to the near-ideal and R–G current related regions of the forward-bias characteristics, respectively.

P: Determine the I_{01}, I_{02}, n_1, and n_2 that provide an optimal match to the forward bias I–V data presented in Fig. 6.10(a).

S: Figure E6.7 is a reproduction of Fig. 6.10(a) with straight lines drawn through the two linear regions on the plot. Based on the generalized modeling expression (and similar to Eq. 6.31), the mathematical description of the straight lines is

$$\ln(I) = \ln(I_{0j}) + \frac{q}{n_j kT}V_A \qquad \ldots j = 1, 2$$

The $V_A = 0$ intercept therefore yields the I_{0j} values, and the n_j-values can be computed from

$$n_j = \frac{V_{A2} - V_{A1}}{(kT/q)\ \ln(I_2/I_1)}$$

where 1 and 2 are any two points along the straight lines. We conclude

$I_{01} \cong 10^{-14}$ A	$n_1 = 1.01$
$I_{02} \cong 10^{-12}$ A	$n_2 = 1.56$

The I_{DIFF} component is almost uncharacteristically ideal. The observed I_{R-G} n-factor is on the low side but within the normally observed range. $I_{02} \gg I_{01}$, as expected.

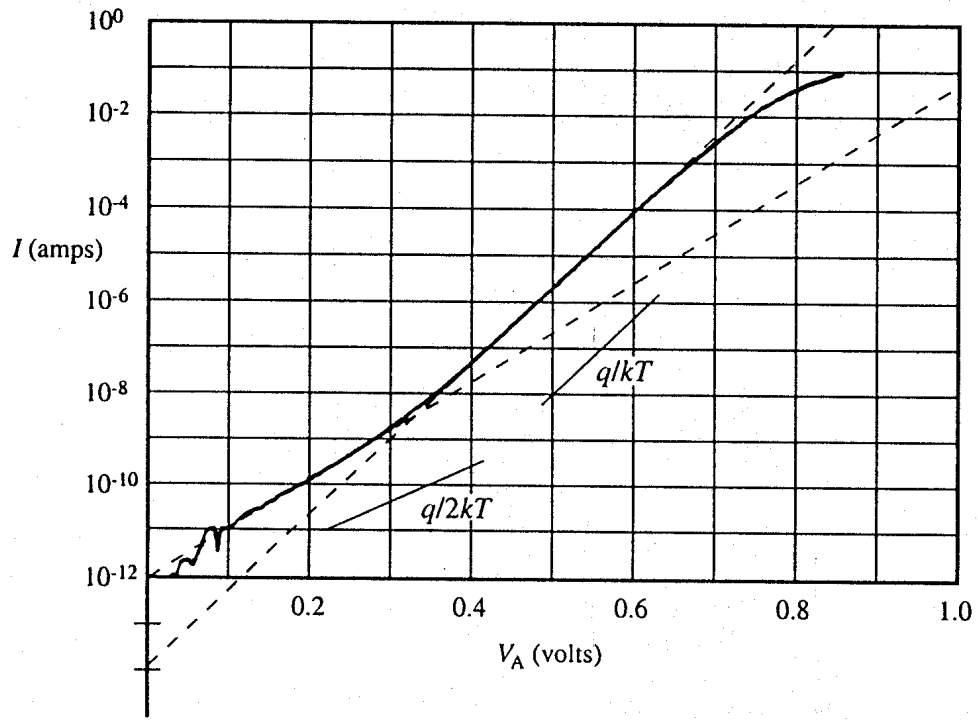

Figure E6.7

6.2.4 $V_A \rightarrow V_{bi}$ High-Current Phenomena

A significant current begins to flow in the diode when the applied forward bias approaches V_{bi}. A large current in turn creates conditions inconsistent with a number of ideal diode assumptions and approximations. For one, the assumption that all of the applied voltage is dropped across the depletion region becomes questionable. If $I = 0.1$ A, for example, a

resistance outside the depletion region of only 1 ohm would give rise to a significant voltage drop of 0.1 V. A large current may also produce a high level of injection. The effects and modeling of these deviations are considered next.

Series Resistance

The quasineutral regions have an inherent resistance determined by the doping and dimensions of the regions. Although quite small in a well-made device, there is also a residual resistance associated with the diode contacts. These combine to form a resistance, R_S, in series with the current flow across the junction as envisioned in Fig. 6.16(a). At low current levels the voltage drop across the series resistance, IR_S, is totally negligible compared to the applied voltage drop across the depletion region better known as the "junction" voltage, V_J. Under the cited condition, $V_J = V_A$, as assumed in the electrostatic and ideal diode

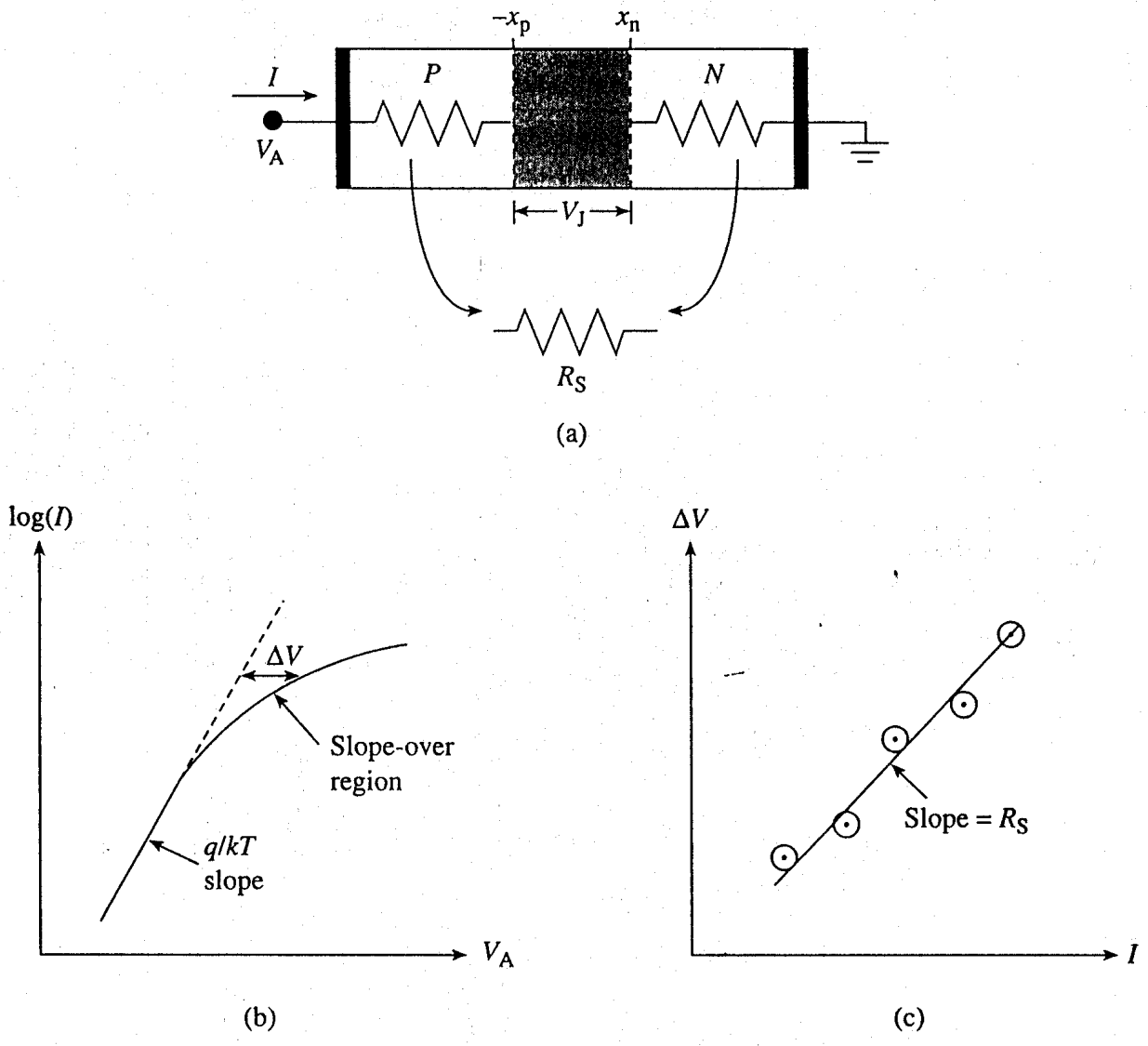

Figure 6.16 Identification and determination of the series resistance. (a) Physical origin of R_S. (b) Forward-bias semilog plot used to deduce ΔV versus I. (c) ΔV versus I plot used to deduce R_S.

derivations. At current levels where IR_S becomes comparable to V_A, however, the applied voltage drop appearing across the depletion region is reduced to

$$\boxed{V_J = V_A - IR_S} \tag{6.48}$$

Effectively, part of the applied voltage is wasted, a larger applied voltage is necessary to achieve the same level of current compared to the ideal, and the characteristics slope over as illustrated in Fig. 6.10(a).

To correct for the series resistance, one merely replaces V_A by $V_J = V_A - IR_S$ in previously derived I–V_A relationships. Since the diffusion current typically dominates at the current levels where IR_S becomes important, we can write

$$I = I_0 e^{qV_J/kT} = I_0 e^{q(V_A - IR_S)/kT} \quad \ldots V_A \rightarrow V_{bi} \tag{6.49}$$

Technically Eq. (6.49) is a transcendental equation that cannot be solved for I as a function of V_A. However, I versus V_A is readily established by choosing a V_J value, computing I from Eq. (6.49), and then computing V_A from Eq. (6.48). The computation does require a knowledge of R_S. R_S can be determined from experimental data as outlined in parts (b) and (c) of Fig. 6.16. Working with a forward-bias semilog plot similar to Fig. 6.10(a), one extends the ideal-diode part of the plot into the slope-over region and notes the ΔV voltage displacement between the two curves as a function of I. Since $\Delta V = V_A - V_J = IR_S$, the slope of the line through a plot of the ΔV versus I data yields R_S.

Exercise 6.8

P: Crudely estimate the series resistance of the diode exhibiting the I–V characteristics presented in Fig. 6.10(a).

S: A blow-up of the slope-over region is needed to produce a decent ΔV versus I plot. We can, however, estimate R_S using the ΔV at a given I. The Fig. 6.10(a) I–V curve terminates at a current of about 80 mA when $V_A = 0.85$ V. Referring to Fig. E6.7, we find that an extension of the q/kT region on the plot passes through 80 mA at roughly 0.78 V. Thus $\Delta V \cong 0.07$ V and $R_S = \Delta V/I \approx 0.07/0.08 \sim 1$ ohm.

High-Level Injection

The low-level injection assumption made in the derivation of the ideal diode equation begins to fail when the minority carrier concentration at the depletion region edge on the lightly doped side of the junction approaches the doping concentration. In Si at room temperature this typically occurs at applied voltages a few tenths of a volt below V_{bi}. A further increase in the applied voltage gives rise to high-level injection. Under high-level injection

both the minority carrier and the majority carrier concentrations adjacent to the depletion region are perturbed, as pictured in Fig. 6.17(a). The majority carrier concentration must increase to maintain approximate charge neutrality in the quasineutral regions. An analysis of high-level injection leads to a predicted current varying roughly as $\exp(q/2kT)$. In other words, one expects a high-current $q/2kT$ region on a semilog plot of the forward bias I–V characteristics as sketched in Fig. 6.17(b). The predicted high-current $q/2kT$ region is seldom observed, however, because it is obscured by the slope-over associated with series resistance. We should note, nonetheless, that the enhanced carrier concentrations as-

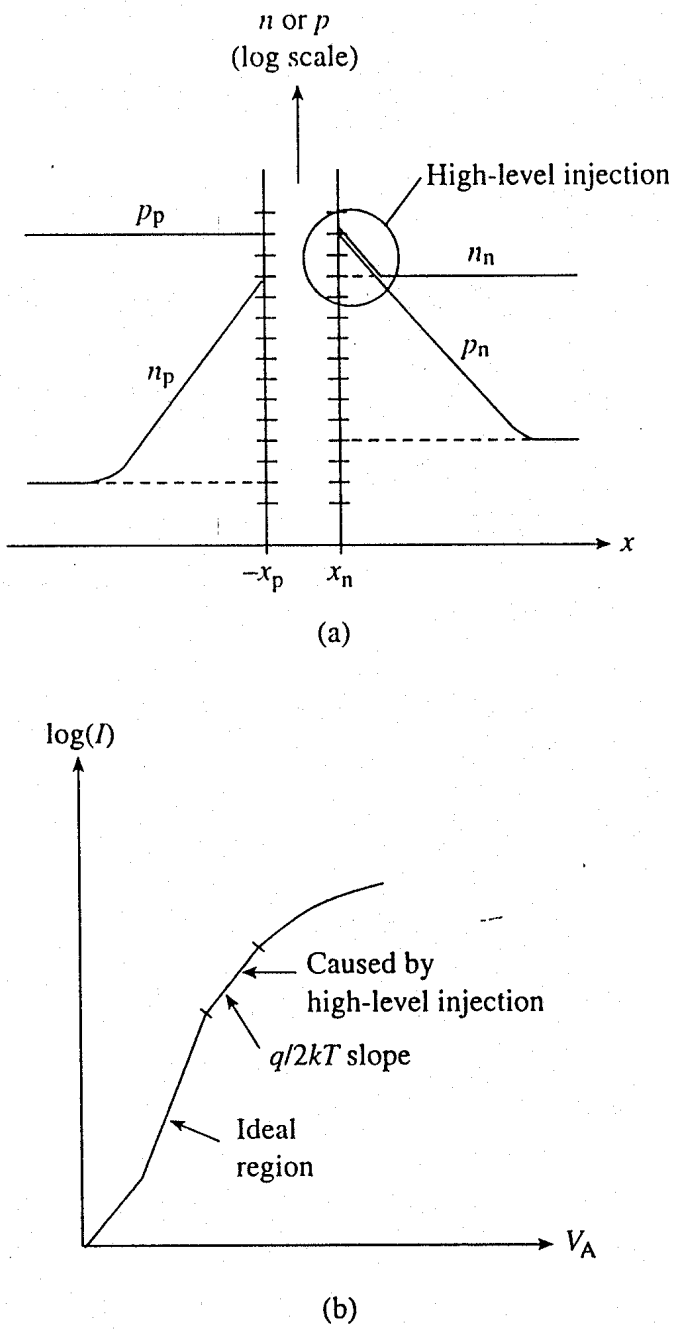

Figure 6.17 High-level injection. (a) Carrier concentrations under high-level injection conditions. (b) Predicted effect on the observed characteristic.

sociated with high-level injection can reduce the observed series resistance. The reduction in resistivity resulting from high levels of carrier injection is referred to as *conductivity modulation.*

Exercise 6.9

P: The measured I–V characteristic of a Si diode maintained at room temperature is crudely sketched in Fig. E6.9. Note that the current scale is logarithmic for forward bias and linear for reverse bias. Nonidealities exhibited by the characteristic are identified by capital letters. Various possible sources for the deviations from the ideal are listed to the right of the sketch. Identify the cause of each nonideal I–V feature; place the proper source number(s) adjacent to the letters on the sketch.

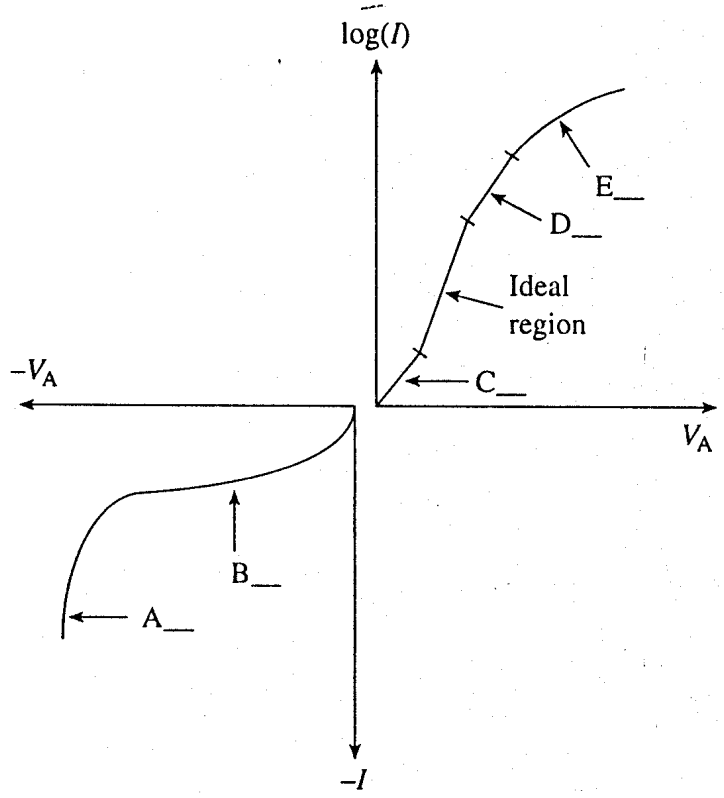

1. Photogeneration
2. Thermal recombination in the depletion region
3. Avalanching and/or Zener process
4. Low-level injection
5. Depletion approximation
6. Thermal generation in the depletion region
7. Band bending
8. Series resistance
9. $V_A > V_{bi}$
10. High-level injection

Figure E6.9

S: A3, B6, C2, D10, E8

6.3 SPECIAL CONSIDERATIONS

The two topics addressed in this section are of a supplemental nature as far as the basic d.c. response of the *pn* junction diode is concerned. Considerations associated with the topics could be delayed until absolutely required later in the text, but that would tend to de-

emphasize their importance by submerging them in a larger context. Also, a linkage of ideas and concepts critical to a greater depth of understanding becomes more difficult to establish. The charge control approach, addressed first, is a sort of "big picture" method of analysis that often allows a reasonably accurate approximate solution with a minimum of mathematics. The narrow-base diode, considered in Subsection 6.3.2, is both a special deviation from the ideal and a conceptual link to the bipolar junction transistor.

6.3.1 Charge Control Approach

In the charge control approach, the basic carrier variable is the charge associated with the minority carrier excess (or deficit) within an entire quasineutral region. To be specific, consider a forward-biased p^+-n junction diode. Let $\Delta p_n(x, t)$ be the minority carrier excess in the n-side quasineutral region at a given time t and at a point x, $x_n \leq x \leq \infty$. The total excess hole charge, Q_P, within the region is then

$$\boxed{Q_P = qA \int_{x_n}^{\infty} \Delta p_n(x, t)\, dx} \tag{6.50}$$

Equation (6.50) also applies to reverse bias with a negative Q_P being interpreted as a carrier deficit. Q_P is of course independent of x, but is potentially a function of time.

Still considering a p^+-n diode, we next seek a relationship that describes the overall behavior of this combined minority carrier charge in the n-side quasineutral region. A logical place to start is the minority carrier diffusion equation, Eq. (3.54b), which describes the overall behavior of the minority carrier hole concentration at a given point. Specifically, with $G_L = 0$,

$$\frac{\partial \Delta p_n}{\partial t} = D_P \frac{\partial^2 \Delta p_n}{\partial x^2} - \frac{\Delta p_n}{\tau_P} \tag{6.51}$$

Since in a $\mathscr{E} \cong 0$ region

$$J_P = -qD_P \frac{\partial \Delta p_n}{\partial x} \tag{6.52}$$

we can alternatively write

$$\frac{\partial (q\Delta p_n)}{\partial t} = -\frac{\partial J_P}{\partial x} - \frac{q\Delta p_n}{\tau_P} \tag{6.53}$$

Being interested in the combined behavior of the $q\Delta p_n(x, t)$, let us integrate all terms in Eq. (6.53) over the volume ($= A \int dx$) of the n-side quasineutral region. After some rearrangement, we arrive at

$$\frac{d}{dt}\left[qA \int_{x_n}^{\infty} \Delta p_n \, dx\right] = -A \int_{J_P(x_n)}^{J_P(\infty)} dJ_P - \frac{1}{\tau_p}\left[qA \int_{x_n}^{\infty} \Delta p_n \, dx\right] \tag{6.54}$$

The bracketed quantities are recognized to be Q_P. Moreover,

$$-A \int_{J_P(x_n)}^{J_P(\infty)} dJ_P = -AJ_P(\infty) + AJ_P(x_n) = AJ_P(x_n) \cong AJ_{DIFF} = i_{DIFF} \tag{6.55}$$

The hole current goes to zero far on the n-side of the junction, making $J_P(\infty) = 0$. Since we are treating a p^+-n junction, $J_{DIFF} = J_N(-x_p) + J_P(x_n) \cong J_P(x_n)$. A lowercase i is used for the final result in Eq. (6.55) because the current is permitted in general to be a function of time. Making the indicated simplifications to Eq. (6.54) yields

$$\boxed{\frac{dQ_P}{dt} = i_{DIFF} - \frac{Q_P}{\tau_p}} \tag{6.56}$$

The result of our manipulations, Eq. (6.56), has a very simple interpretation. It says there are two ways to change the excess hole charge within a region: Holes can flow into or out of the region (i_{DIFF}), or the excess charge can be modified by recombination–generation within the region ($-Q_P/\tau_p$). Eq. (6.56) is effectively a continuity equation for the excess hole charge.

The charge control approach finds application in both steady state and transient analyses. To illustrate its use, consider a p^+-n junction diode under steady state conditions. In the steady state $dQ_p/dt = 0$, $i_{DIFF} = I_{DIFF}$, and Eq. (6.56) reduces to

$$I_{DIFF} = \frac{Q_P}{\tau_p} \tag{6.57}$$

Now suppose a solution was not available for $\Delta p_n(x)$. We do know the value of Δp_n at $x = x_n$ ($x' = 0$) from the Eq. (6.18) boundary condition and we suspect the solution, if obtained, would be exponential with a decay constant of a diffusion length. These facts suggest an approximation similar to that introduced in Exercise 6.4. We equate Q_P to the excess hole charge associated with a squared-off distribution extending a diffusion length

into the n-side and equal to the Δp_n value at the depletion region edge. Therefore, without actually solving for $\Delta p_n(x)$, we estimate

$$Q_P \cong q(AL_P)\Delta p_n(x'=0) = qAL_P\frac{n_i^2}{N_D}(e^{qV_A/kT} - 1) \tag{6.58}$$

giving

$$I_{DIFF} = \frac{Q_P}{\tau_p} = qA\frac{L_P}{\tau_p}\frac{n_i^2}{N_D}(e^{qV_A/kT} - 1) \tag{6.59}$$

Since $L_P/\tau_p = D_P/L_P$, Eq. (6.59) is recognized to be the usual result for the diffusion current in the p^+-n diode.

6.3.2 Narrow-Base Diode

Current Derivation

In the ideal diode derivation the diode contacts were assumed to be several minority carrier diffusion lengths or more from the edges of the depletion region. This gives rise to the $\Delta n_p(-\infty) = 0$ and $\Delta p_n(\infty) = 0$ boundary conditions. For diodes whose width on the lightly doped side is equal to the substrate or wafer thickness, the wide-base diode assumption is typically justified. The assumption comes into question, however, if the diode is fabricated, for example, in a thin epitaxial layer. A diode where the width of the quasineutral region on the lightly doped side of the junction is on-the-order-of or less than a diffusion length is known as a *narrow-base* diode.

To determine the diffusion current flowing in a narrow base diode, it is necessary to revise the ideal diode derivation. We take the diode under analysis to be a p^+-n step junction diode identical in every way to an ideal diode except that the width of the quasineutral n-region is possibly comparable to or less than a minority carrier diffusion length. As graphically defined in Fig. 6.18, x_c is the distance from the metallurgical junction to the n-side contact, and $x_c' = x_c - x_n$ the distance from the n-edge of the depletion region to the n-side contact. The n-side contact is assumed to be ohmic, making $\Delta p_n = 0$ at $x' = x_c'$. In general, the minority carrier concentration at a contact a finite distance from the depletion region edge depends on the rate of carrier recombination–generation at the contact. At a well-made or ohmic contact, the recombination–generation rate is high and the minority carrier concentration is maintained near its equilibrium value.

Paralleling the derivation of the ideal diode equation, we must solve

$$0 = D_P\frac{d^2\Delta p_n}{dx'^2} - \frac{\Delta p_n}{\tau_p} \quad \ldots 0 \le x' \le x_c' \tag{6.60}$$

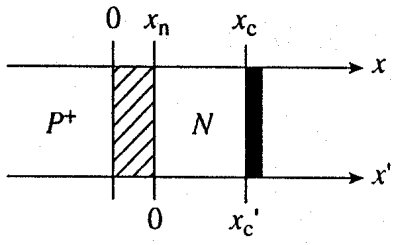

Figure 6.18 Specification of the n-side contact position in a narrow-base diode. x_c' is assumed to be comparable to or less than L_P.

subject to the boundary conditions

$$\Delta p_n(x'=0) = \frac{n_i^2}{N_D}(e^{qV_A/kT} - 1) \tag{6.61a}$$

$$\Delta p_n(x'=x_c') = 0 \tag{6.61b}$$

As in the ideal diode derivation, the general solution is

$$\Delta p_n(x') = A_1 e^{-x'/L_P} + A_2 e^{x'/L_P} \quad \ldots 0 \leq x' \leq x_c' \tag{6.62}$$

Here, however, A_2 is not required to vanish. Rather, applying the boundary conditions gives

$$\Delta p_n(0) = A_1 + A_2 \tag{6.63a}$$

$$0 = A_1 e^{-x_c'/L_P} + A_2 e^{x_c'/L_P} \tag{6.63b}$$

Solving Eqs. (6.63) for A_1 and A_2, and substituting back into the general solution, we conclude

$$\Delta p_n(x') = \Delta p_n(0)\left(\frac{e^{(x_c'-x')/L_P} - e^{-(x_c'-x')/L_P}}{e^{x_c'/L_P} - e^{-x_c'/L_P}}\right) \quad \ldots 0 \leq x' \leq x_c' \tag{6.64}$$

or more compactly in terms of the sinh function

$$\boxed{\Delta p_n(x') = \Delta p_n(0)\frac{\sinh[(x_c'-x')/L_P]}{\sinh[x_c'/L_P]}} \quad \ldots 0 \leq x' \leq x_c' \tag{6.65}$$

where

$$\sinh(\xi) \equiv \frac{e^{\xi} - e^{-\xi}}{2} \tag{6.66}$$

Finally,

$$I_{\text{DIFF}} \cong AJ_{\text{P}}(x' = 0) = -qAD_{\text{P}} \frac{d\Delta p_{\text{n}}}{dx'}\bigg|_{x'=0} \tag{6.67}$$

leading to

$$\boxed{I_{\text{DIFF}} = I_0'(e^{qV_{\text{A}}/kT} - 1)} \tag{6.68}$$

$$\boxed{I_0' \equiv qA \frac{D_{\text{P}}}{L_{\text{P}}} \frac{n_{\text{i}}^2}{N_{\text{D}}} \frac{\cosh(x_{\text{c}}'/L_{\text{P}})}{\sinh(x_{\text{c}}'/L_{\text{P}})}} \tag{6.69}$$

where

$$\cosh(\xi) \equiv \frac{e^{\xi} + e^{-\xi}}{2} \tag{6.70}$$

Limiting Cases/Punch-Through

To assist in the examination and interpretation of results, it is useful to note

$$\sinh(\xi) \rightarrow \begin{cases} \xi & \ldots \xi \rightarrow 0 \quad (6.71a) \\ \dfrac{e^{\xi}}{2} & \ldots \xi \rightarrow \infty \quad (6.71b) \end{cases}$$

$$\cosh(\xi) \rightarrow \begin{cases} 1 + \dfrac{\xi^2}{2} & \ldots \xi \rightarrow 0 \quad (6.72a) \\ \dfrac{e^{\xi}}{2} & \ldots \xi \rightarrow \infty \quad (6.72b) \end{cases}$$

Consider first the limit where $x_{\text{c}}' \rightarrow \infty$. If $x_{\text{c}}' \rightarrow \infty$ or $x_{\text{c}}'/L_{\text{P}} \gg 1$, the ratio of the sinh terms in Eq. (6.65) simplifies to $\exp(-x'/L_{\text{P}})$ and Eq. (6.65) reduces to Eq. (6.23) in the ideal diode derivation. Similarly, $\cosh(x_{\text{c}}'/L_{\text{P}})/\sinh(x_{\text{c}}'/L_{\text{P}}) \rightarrow 1$, and Eq. (6.69) reduces to the standard ideal diode result for a p^+-n junction. In essence, the narrow-base diode analysis may be viewed as a generalization of the ideal diode formulation valid for quasineutral regions of arbitrary thickness.

Although mathematically reassuring, the wide-base limit leads to nothing new. It is the opposite limit where $x_c' \to 0$ that proves to be more interesting. For one, if $x_c'/L_P \ll 1$, the sinh terms in Eq. (6.65) can be replaced by their arguments, and $\Delta p_n(x')$ dramatically simplifies to

$$\Delta p_n(x') = \Delta p_n(0)\left(1 - \frac{x'}{x_c'}\right) \tag{6.73}$$

The perturbed carrier concentration becomes a linear function of position, just a straight line connecting the two endpoint values set by the boundary conditions. The linear dependence is a direct consequence of negligible thermal recombination–generation in a region much shorter than a diffusion length. In fact, the Eq. (6.73) result could have been obtained much more readily by neglecting the R–G term $(-\Delta p_n/\tau_p)$ in the original minority carrier diffusion equation. This observation is justification for henceforth *neglecting the thermal R–G term in the minority carrier diffusion equation when the quasineutral width is small compared to a diffusion length.*

A second small-width observation involves the reverse-bias current. In the limit where $x_c'/L_P \ll 1$, $\cosh(x_c'/L_P)/\sinh(x_c'/L_P) \to L_P/x_c'$ and $I_0' \to qA(n_i^2/N_D)(D_P/x_c')$. The width of the quasineutral region, $x_c' = x_c - x_n$, decreases with increasing reverse bias because of the growing depletion width. It therefore follows that $I_{DIFF}(V_A < 0) \cong -I_0' \propto 1/x_c'$ does not saturate, but systematically increases with the applied reverse bias. If x_c is sufficiently small, there is also the possibility of $x_c' \to 0$. The situation where an entire device region becomes depleted is referred to as *punch-through.* Based on the Eq. (6.68)/(6.69) result, $I_{DIFF}(V_A < 0) \to -\infty$ if $x_c' \to 0$. However, because of the depletion approximation used in defining the width and nature of the quasineutral region, the theoretical formulation becomes invalid in the extreme $x_c' \to 0$ limit. Experimentally and in more precise theoretical formulations, the diffusion current remains finite at the punch-through voltage in a narrow-base diode, provided the electric field inside the device is insufficient to produce avalanche breakdown.

Exercise 6.10

P: A planar Si p^+-n step junction diode maintained at room temperature has an n-side doping of $N_D = 10^{16}/\text{cm}^3$ and an n-side thickness of $x_c = 2\ \mu\text{m}$. Invoking the depletion approximation, determine the punch-through voltage; i.e., determine the voltage required to completely deplete the n-side of the diode.

S: At the punch-through voltage $x_n = x_c$, where from Eq. (5.37),

$$x_n \cong \left[\frac{2K_S\varepsilon_0}{qN_D}(V_{bi} - V_A)\right]^{1/2}$$

Thus

$$x_n^2 = x_c^2 = \frac{2K_S\varepsilon_0}{qN_D}(V_{bi} - V_A)$$

$$V_A = V_{bi} - \frac{qN_D}{2K_S\varepsilon_0}x_c^2$$

$$= 0.92 - \frac{(1.6 \times 10^{-19})(10^{16})(2 \times 10^{-4})^2}{(2)(11.8)(8.85 \times 10^{-14})} = \mathbf{-29.7\ V}$$

V_{bi} was read from Fig. E5.1 in Subsection 5.1.4.

Inspecting Fig. 6.11, we note that avalanche breakdown occurs at $V_{BR} \cong 55$ V in a comparable wide-base diode. Thus, punch-through will take place prior to breakdown in the given narrow-base diode.

6.4 SUMMARY AND CONCLUDING COMMENTS

The chapter was devoted to modeling the steady state response of the *pn* junction diode. We began with a qualitative description of diode operation using the energy band diagram as a visualization tool. The reverse-bias current in an ideal diode is associated with minority carriers wandering into the depletion region and being accelerated to the opposite side of the junction. Forward biasing lowers the potential hill between the two sides of the diode and enhances majority carrier injection across the junction and into the opposite-side quasineutral region. There is of course no carrier build-up anywhere inside the device under steady state conditions. Recombination–generation acts to stabilize the minority carrier concentrations, while a very rapid rearrangement and interchange with the contacts maintain the constancy of the majority carrier concentrations.

Considerable attention was next given to the formulation, derivation, and examination of the ideal diode theory. Although the predicted *I–V* characteristic exhibits serious deficiencies when carefully compared with experiment, the ideal diode development provides valuable insight into the internal operation of the diode and an analytical base for more accurate formulations. Even with its limitations, the theory and extensions of the theory are widely used in diode and other device analyses to obtain manageable first order predictions. The ideal diode equation, it should be cautioned, is only a small part of the ideal diode theory. The theory encompasses a clear understanding of the solution strategy and approximations, the mathematical steps to follow in establishing a quantitative result, and predictions relative to carrier concentrations, carrier currents, material dependencies, doping dependencies, and so on.

As already acknowledged, a careful comparison between the ideal diode and experi-

mental I–V characteristics revealed several deviations from the ideal. For a Si diode maintained at room temperature, the deviations included reverse-bias breakdown, excess current levels under small forward bias and all reverse biases, and a reduced I–V slope or slope-over at forward biases approaching V_{bi}. Breakdown was associated with avalanching or the Zener process, the excess current with thermal carrier recombination–generation in the depletion region, and the reduced I–V slope at high forward currents with the voltage drop across internal series resistances or possibly high-level injection. Each of the deviation-causing phenomena was described physically, and the more important phenomena were modeled analytically. Information of special note included V_{BR} due to avalanching varies roughly as the inverse of the doping concentration on the lightly doped side of the junction, carrier multiplication leads to an enhanced current far below the breakdown voltage, the R–G current exhibits an expected dependence approaching $\exp(qV_A/2kT)$ under forward biasing and is proportional to W under reverse biasing, the R–G current varies as n_i while the diffusion current varies as n_i^2, the voltage drop across the internal series resistance reduces the voltage drop across the junction to $V_J = V_A - IR_S$, and high-level injection gives rise to an expected high-current $\exp(qV_A/2kT)$ operational region that is usually obscured by the slope-over associated with series resistance. The development, it should be noted, concentrated on the step junction. Analytical modifications may be required in treating other profiles.

In the special considerations section we introduced an analytical approach known as charge control and generalized the ideal diode analysis to accommodate base widths of arbitrary thickness. When the quasineutral width is small compared to a diffusion length, the perturbed carrier distribution was noted to become linear. For extremely small base widths, there is also the possibility of punch-through or complete depletion of the narrow base at a reverse-bias voltage less than V_{BR}.

Although we have covered the highlights in this summary, there are other pieces of information—terms, techniques, approximations, equations—that are part of the overall information package. The Part II Supplement and Review does contain a Review List of Terms grouped by chapter. As far as equations are concerned, the ideal diode solution (Eqs. 6.29/6.30), the law of the junction (Eq. 6.12), the depletion-edge boundary conditions (Eqs. 6.15/6.18), and the reverse-bias R–G current expression (Eq. 6.43) might be committed to memory. The book should be retained for looking up the remainder of the equations.

PROBLEMS

CHAPTER 6 PROBLEM INFORMATION TABLE

Problem	*Complete After*	*Difficulty Level*	*Suggested Point Weighting*	*Short Description*
6.1	6.1.4	1	10 (1 each part)	Ideal diode quiz
6.2	6.2.4	1	10	Compare actual-ideal I–V

6.3	6.1.1	1	9 (3 each part)	Band diagram sketches
6.4	"	2	8	Forward-bias big picture
6.5	6.1.2	2–3	10	Derive Eq. (6.15) using $J_N=0$
●6.6	6.1.3	2	10 (5 each part)	Typical I values using `diary`
●6.7	"	2	16 (a-10, b-5, c-1)	Ideal I–V variation with T
6.8	"	3	16 (a-3, b-10, c-3)	Photodiode I–V derivation
●6.9	"	1	5	Photodiode I–V plot
6.10	6.1.4	2	10 (a::c-2, d-4)	Deduce info from conc. plot
6.11	"	3	12	Deduce, plot carrier conc.
●6.12	"	3	12 (a-9, b-3)	*pn* diode T-sensor
6.13	6.2.2	2	6 (2 each part)	V_{BR}-related calculations
●6.14	"	2	10 (a-8, b-2)	Breakdown I–V (MI_0)
●6.15	6.2.3	3	12	Breakdown I–V ($MI_{R\text{-}G}$)
6.16	"	3	8	Determine elevated T-point
6.17	"	3	10	Modified $I_{R\text{-}G}$
6.18	6.2.4	3	9 (a-6, b-3)	R_S-related computations
6.19	"	3	20 (10-line fit, 8-least sq. fit, 2-discuss)	Deduce I_{0j}, n_j from I–V
6.20	"	2–3	15	Deduce R_S from I–V
●6.21	"	4	40 (a-2, b-10, c::e-8, f-4)	Multiple nonideality I–V
6.22	6.3.2	3	10	Pseudo-narrow-base diode
6.23	"	3	15	Narrow/wide diode combo
6.24	"	4	34 (a-2, b-2, c-4, d-2, e-12, f-12)	Multiple considerations

6.1 Ideal Diode Quiz

Answer the following questions as concisely as possible. Assume the questions refer to an ideal diode.

(a) The forward-bias current is associated with what type of carrier activity?

(b) The reverse-bias current is associated with what type of carrier activity?

(c) Why is the reverse-bias current expected to be small in magnitude and to saturate at a small reverse voltage?

(d) Under reverse biasing, what processes occur in the quasineutral regions adjacent to the depletion region edges? Is it drift and diffusion, diffusion and recombination, generation and diffusion, or generation and drift?

(e) Why can't the minority carrier diffusion equations be used to determine the minority carrier concentrations and currents in the depletion region of a diode?

(f) What a priori justification is there for assuming recombination–generation is negligible throughout the depletion region?

(g) What exactly is a "wide-base" diode?

(h) What is the "law of the junction"?

(i) Given a semilog plot of the forward bias I–V characteristic, how does one determine I_0?

(j) True or false: The reverse-bias saturation current may be alternatively viewed as arising from minority carrier generation in the quasineutral regions.

6.2 Compare (preferably with the aid of sketches) the I–V characteristic derived from an actual Si *pn* junction diode maintained at room temperature and the theoretical ideal-diode characteristic. In effecting your comparison, carefully note and (as necessary) clarify all deviations from the ideal. Finally, briefly identify the cause of each deviation from the ideal theory. Devote no more than a sentence or two to the cause of each deviation.

6.3 Sketch the energy band diagram for an ideal p^+-n step junction diode showing the carrier activity in and near the depletion region when

(a) $V_A = 0$.

(b) $V_A > 0$.

(c) $V_A < 0$.

6.4 Construct a composite energy-band/circuit diagram analogous to Fig. 6.2 that provides an overall view (the "big picture" view) of carrier activity inside a *forward-biased pn* junction diode.

6.5 Referring to the V_{bi} derivation in Subsection 5.1.4, show that the Eq. (6.15) boundary condition can be derived by continuing to assume $J_N = 0$ when $V_A \neq 0$. Use the Eq. (5.10) result to eliminate V_{bi} in your expression for $n(-x_p)$.

• **6.6** Considering an n^+-p silicon step junction ($N_A = 10^{15}/\text{cm}^3$, $\tau_n = 10^{-6}$ sec, $A = 10^{-3}$ cm^2) to be ideal, perform calculations to determine typical current levels expected from the device under different temperature and biasing conditions. Invoke the MATLAB `diary` function to record your work.

(a) Compute the ideal diode current at $T = 300$ K when (i) $V_A = -50$ V, (ii) $V_A = -0.1$ V, (iii) $V_A = 0.1$ V, and (iv) $V_A = 0.5$ V.

(b) Assuming τ_n does not vary significantly with temperature, repeat part (a) for $T = 500$ K.

• **6.7** In this problem we wish to explore how the ideal diode I–V characteristic varies as a function of temperature. Consider an ideal Si p^+-n step junction diode with an area $A = 10^{-4}$ cm^2, $N_D = 1.0 \times 10^{16}$/cm^3, and a room temperature $\tau_p = 10^{-6}$ sec.

(a) Using the empirical-fit relationship for the hole mobility specified in Exercise 3.1, the n_i fit relationship cited in Exercise 2.4(b), and assuming τ_p to be temperature-independent, construct a MATLAB program that computes and plots the ideal I–V characteristic of the diode with temperature T in Kelvin being considered an input variable. Print out a sample plot simultaneously displaying the characteristics associated with $T = 295$ K, 300 K, and 305 K. (To clearly display both the reverse and forward characteristics, limit the plot axes to -1 V $\leq V_A \leq 0.2$ V and $-2I_0 \leq I \leq 5I_0$. Use the largest I_0 to set the current limits when displaying several I–V curves on the same set of coordinates.)

(b) Appropriately modify your part (a) program to obtain a semilog plot of I_0 versus T for 300 K $\leq T \leq$ 400 K.

(c) Comment on the part (a) and (b) results.

6.8 Photodiode/Solar Cell

A *pn* junction photodiode is just a *pn* junction diode that has been specially fabricated and encapsulated to permit light penetration into the vicinity of the metallurgical junction. Commercially available solar cells are in essence large-area *pn* junction photodiodes designed to minimize energy losses. The general form of the similar I–V characteristics exhibited by photodiodes and solar cells is readily established by a straightforward modification of the ideal diode equation.

Consider an ideal p^+-n step junction diode where incident light is uniformly absorbed throughout the device producing a photogeneration rate of G_L electron-hole pairs per cm^3-sec. Assume that low-level injection prevails.

(a) What is the excess minority carrier concentration on the n-side a large distance ($x \rightarrow \infty$) from the metallurgical junction. [NOTE: $\Delta p_n(x \rightarrow \infty) \neq 0$.]

(b) The usual ideal diode boundary conditions (Eqs. 6.15 and 6.18) still hold at the edges of the depletion region. Using the revised boundary condition established in part (a) and Eq. (6.18), derive an expression for the I–V characteristic of the p^+-n diode under the stated conditions of illumination. As in the derivation of the ideal diode equation, ignore all recombination–generation, including photogeneration, occurring in the depletion region.

(c) Sketch the general form of the photodiode I–V characteristics taking in turn $G_L = 0$, $G_L = G_{L0}$, $G_L = 2G_{L0}$, and $G_L = 4G_{L0}$. Assume the light intensity is high enough to significantly perturb the characteristics when $G_L = G_{L0}$. (NOTE: Problem 6.9 can be substituted for this part of the problem.)

• **6.9** *I–V* characteristics of a solar cell are approximately modeled by the relationship,

$$I = I_0(e^{qV_A/kT} - 1) + I_L$$

where I_L is the current due to light. I_L is always negative and a voltage-independent constant for a given level of illumination. Construct a plot illustrating the general nature of the solar cell characteristics. Setting $T = 300$ K, simultaneously plot I/I_0 versus V_A for the assumed values of $I_L/I_0 = 0, -1, -2$, and -4. Limit V_A to $-0.5\text{ V} \leq V_A \leq 0.1\text{ V}$.

6.10 Figure P6.10 is a dimensioned plot of the steady state carrier concentrations inside a *pn* step junction diode maintained at room temperature.

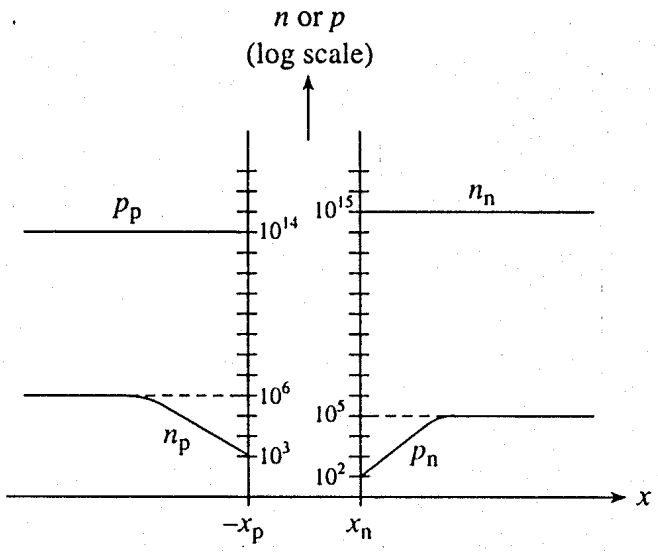

Figure P6.10

(a) Is the diode forward or reverse biased? Explain how you arrived at your answer.

(b) Do low-level injection conditions prevail in the quasineutral regions of the diode? Explain how you arrived at your answer.

(c) What are the *p*-side and *n*-side doping concentrations?

(d) Determine the applied voltage, V_A.

6.11 A voltage $V_A = 23.03(kT/q)$ is being applied to a step junction diode with *n*- and *p*-side dopings of $N_A = 10^{17}/\text{cm}^3$ and $N_D = 10^{16}/\text{cm}^3$, respectively. $n_i = 10^{10}/\text{cm}^3$. Make a dimensioned log(*p* and *n*) versus *x* sketch of both the majority and minority carrier concentrations in the quasineutral regions of the device. Identify points 10 and 20 diffusion lengths from the depletion region edges on your sketch.

• **6.12** As was confirmed graphically in Problem 6.7, the I–V characteristics of the *pn* junction diode are very sensitive to temperature. It should not be too surprising then that there are silicon diodes sold commercially as temperature sensors. To use the diode to measure temperature, it is typically forward-biased with a constant current source and V_A is monitored as a function of T as shown in Fig. P6.12. Make the assumption the diode is being operated in the forward bias range where $I \cong I_0 \exp(qV_A/kT)$. Also take the intended range of operation to be $0 \leq T(^\circ\text{C}) \leq 100^\circ\text{C}$.

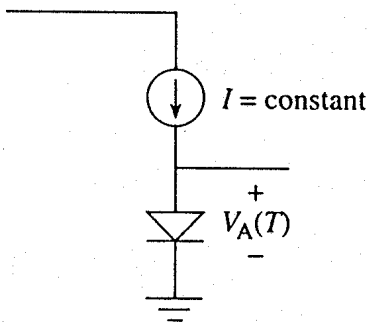

Figure P6.12

(a) With I as an input variable, modify the Problem 6.7(b) program to compute and plot V_A versus T for $0 \leq T(^\circ\text{C}) \leq 100^\circ\text{C}$. Print out a sample plot using $I = 10^{-4}$ A.

(b) Considering the sensitivity (dV_A/dT in mV/°C) of the sensor, would it be preferable to monitor the temperature using $I = 10^{-4}$ A or $I = 10^{-3}$ A? Support your answer.

6.13 Given a planar p^+-n Si step junction diode with an n-side doping of $N_D = 10^{15}/\text{cm}^3$ and $T = 300$ K, determine

(a) The approximate V_{BR} of the diode.

(b) The depletion width at the breakdown voltage.

(c) The maximum magnitude of the electric field in the depletion region at the breakdown voltage.

• **6.14** Let us pursue the modeling of carrier multiplication and avalanche breakdown in an otherwise ideal diode. As noted in the text, Eq. (6.35) can be used to correct the ideal diode equation and approximately account for carrier multiplication. I_0 is simply replaced by MI_0. Moreover, the expected V_{BR} due to avalanching varies roughly as $N_B^{-0.75}$. A reasonable fit to the Fig. 6.11 dependence for Si diodes is

$$V_{BR} \cong 60(N_B/10^{16})^{-0.75}$$

where N_B is in cm^{-3} and V_{BR} is in volts. Take the Si diode under analysis to be a nearly ideal p^+-n step junction maintained at 300 K.

(a) Construct a MATLAB program to perform I–V computations that include carrier multiplication and avalanche breakdown. Specifically, compute and plot the modified reverse bias I/I_0 versus V_A characteristic covering the range from $-V_{BR}$ to 0. (Note the I_0 normalization.) Employ $m = 6$ in your computations and set the `axis` function parameters to $[-1.1*V_{BR}, 0, -5, 0]$. Print out a sample characteristic taking $N_D = 2 \times 10^{16}/cm^3$. Is your plot consistent with the curving approach to breakdown shown in Fig. 6.10(b) and Exercise 6.5?

(b) Use your program to explore how the diode characteristic varies as a function of m and the impurity concentration on the lightly doped side of the junction.

• **6.15** Repeat Problem 6.14 replacing I_0 by the reverse bias I_{R-G}. Normalize the current axis to the magnitude of the current at $V_A = -V_{BR}/2$. Run your program setting $N_D = 2 \times 10^{16}/cm^3$. Compare your plot with Fig. 6.10(b).

6.16 The diffusion component of the current is expected to dominate in Si diodes at sufficiently elevated temperatures. What is a sufficiently elevated temperature? To answer this question, suppose one has a Si p^+-n step junction diode where $N_D = 10^{16}/cm^3$, $\tau_0 = \tau_p$, and $L_P \cong 10^{-2}$ cm for 300 K $\leq T \leq$ 500 K. Determine the temperature where $I_{DIFF} = I_{R-G}$ at a reverse bias of $V_{bi} - V_A = V_{BR}/2$.

6.17 Inside a Si diode at 300 K a region of width d contains *three times as many R–G centers* as adjoining regions. This special region, as envisioned in Fig. P6.17, lies totally inside the depletion region when the diode is zero biased. Derive an expression for the R–G current (I_{R-G}) to be expected from the diode when reverse-biased greater than a few kT/q volts. Record all derivational steps.

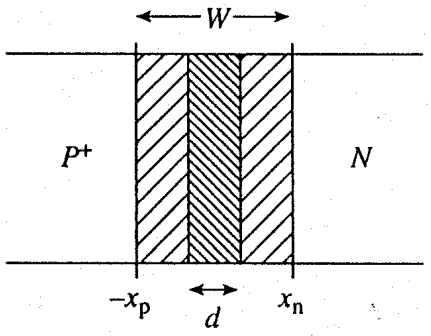

Figure P6.17

6.18 Suppose $I_0 = 10^{-14}$ A and $R_S = 2\ \Omega$ in a diode where high-level injection is negligible. $T = 300$ K.

(a) Determine the forward-bias current at which the applied voltage differs from the ideal by 10%.

(b) Repeat part (a) with $R_S = 20\ \Omega$

6.19 Point-by-point forward-bias I–V data from a 1N757 Si *pn* junction diode maintained at room temperature is listed in Table P6.19 and plotted in Fig. P6.19. Following the procedure outlined in Exercise 6.7, determine I_{01}, I_{02}, n_1, and n_2. Because the line-drawing approach is somewhat subjective, also apply a least squares fit (available in MATLAB) to appropriate segments of the data to determine the fit parameters. Discuss your results.

Table P6.19

V_A (volts)	I (amps)	V_A (volts)	I (amps)
0.02	6.070×10^{-10}	0.48	3.615×10^{-6}
0.04	1.203×10^{-9}	0.50	5.200×10^{-6}
0.06	2.165×10^{-9}	0.52	7.576×10^{-6}
0.08	3.508×10^{-9}	0.54	1.122×10^{-5}
0.10	5.417×10^{-9}	0.56	1.711×10^{-5}
0.12	8.210×10^{-9}	0.58	2.694×10^{-5}
0.14	1.183×10^{-8}	0.60	4.426×10^{-5}
0.16	1.730×10^{-8}	0.62	7.587×10^{-5}
0.18	2.449×10^{-8}	0.64	1.359×10^{-4}
0.20	3.416×10^{-8}	0.66	2.531×10^{-4}
0.22	4.764×10^{-8}	0.68	4.852×10^{-4}
0.24	6.501×10^{-8}	0.70	9.444×10^{-4}
0.26	8.866×10^{-8}	0.72	1.841×10^{-3}
0.28	1.209×10^{-7}	0.74	3.518×10^{-3}
0.30	1.666×10^{-7}	0.76	6.433×10^{-3}
0.32	2.305×10^{-7}	0.78	1.103×10^{-2}
0.34	3.201×10^{-7}	0.80	1.752×10^{-2}
0.36	4.462×10^{-7}	0.82	2.585×10^{-2}
0.38	6.285×10^{-7}	0.84	3.579×10^{-2}
0.40	8.845×10^{-7}	0.86	4.706×10^{-2}
0.42	1.249×10^{-6}	0.88	5.941×10^{-2}
0.44	1.776×10^{-6}	0.90	7.264×10^{-2}
0.46	2.527×10^{-6}		

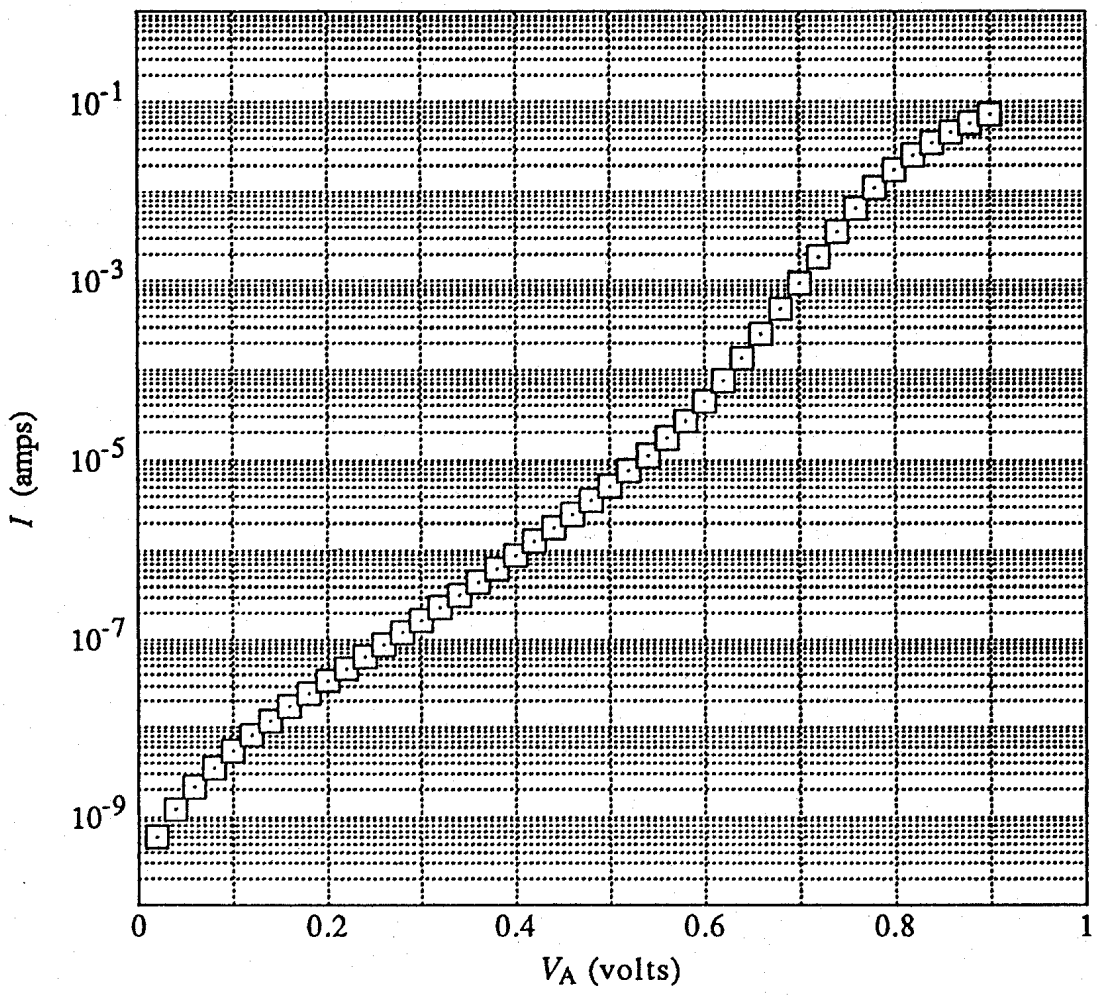

Figure P6.19

6.20 Following the procedure outlined in Fig. 6.16, determine the R_S value of the 1N757 diode characterized by the room temperature data listed in Table P6.19 and plotted in Fig. P6.19.

• **6.21** The model shown in Fig. P6.21 is sometimes employed as a generalized representation of real *pn* junction diodes. The diode symbol is understood to represent the standard model of the device including the diffusion and R–G components of the junction current. The series resistor (R_S) accounts for non-negligible voltage drops in the quasineutral regions and contacts of the diode under high-current conditions. The shunt resistor (R_{SH}) accounts for a possible leakage current in the semiconductor external to the *pn* junction. Note that the current through the *pn* junction and the voltage drop across the junction are redefined to be I_J and V_J, respectively.

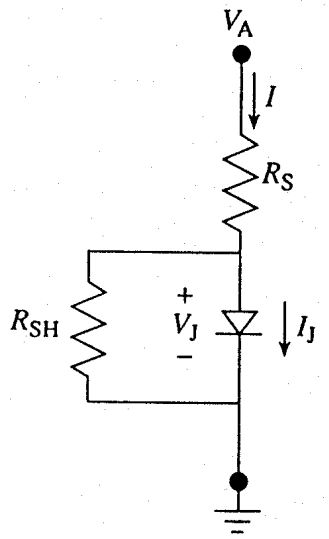

Figure P6.21

(a) If the current through the junction proper is described by the relationship,

$$I_J = I_{01}(e^{qV_J/n_1kT} - 1) + I_{02}(e^{qV_J/n_2kT} - 1)$$

where I_{01} and I_{02} are constants and typically $n_1 \cong 1$ and $n_2 \cong 2$, confirm that the total current through the diode is described by

$$I = I_{01}(e^{qV_J/n_1kT} - 1) + I_{02}(e^{qV_J/n_2kT} - 1) + \frac{V_J}{R_{SH}}$$

with $V_A = V_J + IR_S$

(b) Construct a computer program that can be used to investigate the effect of R_S, R_{SH}, and the size of the current prefactors (I_{01} and I_{02}) on the shape of the observed *forward-bias* I–V_A characteristic. In performing the computation, it is best to obtain I–V_A data pairs associated with evenly stepped values of V_J. Limit your plotted log(I) vs. V_A output to $0 \leq V_A \leq 1$ V and 10^{-10} A $\leq I \leq 10^{-2}$ A. Employ $I_{01} = 10^{-13}$ A, $I_{02} = 10^{-9}$ A, $n_1 = 1$, $n_2 = 2$, $R_S = 1\ \Omega$, $R_{SH} = 10^{12}\ \Omega$, and $T = 300$ K in your initial calculation.

(c) Employing a manually controlled computational switch, modify your program so that it computes and *simultaneously* displays four I–V_A characteristics associated with four different values of *either* R_{SH}, R_S, I_{01}, or I_{02}. Using the same basic set of parameters as specified in part (b), compute and record the I–V_A characteristics resulting from the following variation of parameters:

(i) $R_{SH} = 10^{12}$, 10^9, 10^6, and $10^3\ \Omega$ ($I_{01} = 10^{-13}$ A, $I_{02} = 10^{-9}$ A, $R_S = 1\ \Omega$);

(ii) $R_S = 1$, 10, 10^2, and $10^3\ \Omega$ ($I_{01} = 10^{-13}$ A, $I_{02} = 10^{-9}$ A, $R_{SH} = 10^{12}\ \Omega$);

(iii) $I_{02} = 10^{-9}$, 10^{-10}, 10^{-11}, and 10^{-12} A ($I_{01} = 10^{-13}$ A, $R_S = 1\ \Omega$, $R_{SH} = 10^{12}\ \Omega$);

(iv) $I_{01} = 10^{-13}$, 10^{-12}, 10^{-11}, and 10^{-10} A ($I_{02} = 10^{-9}$ A, $R_S = 1\ \Omega$, $R_{SH} = 10^{12}\ \Omega$).

(d) Following the procedure established in Exercise 6.6, construct a subsidiary program that can be used to compute I_{01} and I_{02} from first principle relationships. Specifically assume a n^+-p step junction. Join the subsidiary program to your main program and obtain sample results employing $A = 10^{-2}$ cm^2, $N_A = 10^{15}$/cm^3, and $\tau_n = \tau_p = \tau_0 = 10^{-6}$ sec. The remainder of the parameters should of course be appropriate for Si at $T = 300$ K.

(e) Construct a modified version of the part (c) program that displays the computed results on a *linear* I–V_A plot. Limit the linear current axis to $0 \leq I \leq 10^{-2}$ A. Compute and record linear plots of the I–V_A characteristics resulting from the variation of parameters specified in part (c). How do the results here compare with those obtained in part (c)?

(f) Generally comment on the results obtained in this problem.

6.22 Consider the special silicon p^+-n step junction diode pictured in Fig. P6.22. Note that $\tau_p = \infty$ for $0 \leq x \leq x_b$ and $\tau_p = 0$ for $x_b \leq x \leq x_c$. Excluding biases that would cause high-level injection or breakdown, develop an expression for the room-temperature I–V characteristic of the diode. Assume the depletion width (W) never exceeds x_b for all biases of interest.

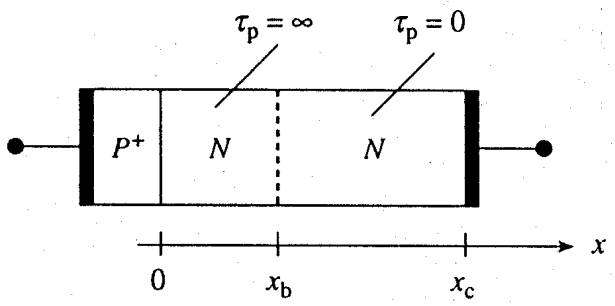

Figure P6.22

6.23 Reconsider the special silicon p^+-n junction diode pictured in Fig. P6.22. Instead of $\tau_p = 0$ in the $x_b \leq x \leq x_c$ region, take τ_p to be nonzero but still sufficiently small so that $L_P \ll x_c - x_b$. Assuming the depletion width (W) never exceeds x_b for all biases of interest, and excluding biases that would cause high-level injection or breakdown, derive an expression for the room temperature I–V characteristic of the diode.

6.24 In modern device processing a procedure called *denuding* is used to reduce the R–G center concentration in the near-surface region of devices. A planar Si p^+-n step junction diode maintained at 300 K has an n-side doping of $N_D = 10^{16}$/cm^3. As shown in Fig. P6.24, denuding has created a reduced R–G center concentration of N_{T1} in the n-side

region from $x = 0$ to $x = x_b = 2\ \mu$m. The R–G center concentration in the $x > x_b$ n-side region is $N_{T2} = 100N_{T1}$.

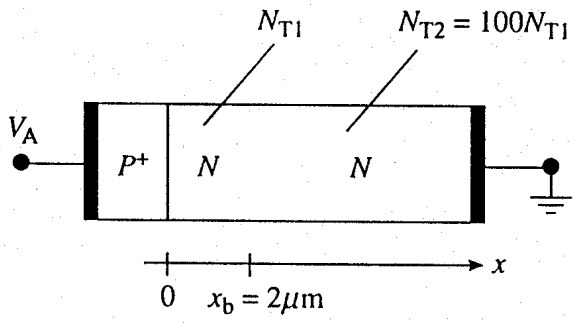

Figure P6.24

(a) What is the junction built-in voltage (V_{bi})?

(b) What is the diode breakdown voltage (V_{BR})?

(c) What applied voltage is necessary to expand the n-side depletion region edge to $x = x_b$?

(d) If the minority carrier lifetimes are τ_{p1} and τ_{p2} in the near-junction and $x > x_b$ regions, respectively, what is the τ_{p1}/τ_{p2} ratio?

(e) Establish an expression or expressions for the diffusion current (I_{DIFF}) flowing in the diode as a function of the applied voltage. To simplify the development, assume $L_{P1} \gg x_b$ and take the n-side contact to be many L_{P2} diffusion lengths from the depletion region edge. Make a sketch of the expected I_{DIFF} versus V_A characteristic when the diode is reverse-biased.

(f) Assuming $\tau_{01} \cong \tau_{p1}$ for $0 \leq x \leq x_b$ and $\tau_{02} \cong \tau_{p2}$ for $x > x_b$, establish an expression or expressions for the R–G current (I_{R-G}) as a function of the applied voltage when the diode is reverse-biased greater than a few kT/q volts. Make a sketch of the expected reverse-bias I_{R-G} versus V_A characteristic.